NASA MEMO 2-2-59H

MEMORANDUM

FLIGHT-DETERMINED STABILITY AND CONTROL DERIVATIVES OF A SUPERSONIC AIRPLANE WITH A LOW-ASPECT-RATIO UNSWEPT WING AND A TEE-TAIL

By William H. Andrews and Herman A. Rediess

High-Speed Flight Station
Edwards, Calif.

NATIONAL AERONAUTICS AND SPACE ADMINISTRATION

WASHINGTON

April 1959

Code - 1

Copy # 1

NATIONAL AERONAUTICS AND SPACE ADMINISTRATION

MEMORANDUM 2-2-59H

FLIGHT-DETERMINED STABILITY AND CONTROL DERIVATIVES OF A SUPERSONIC AIRPLANE WITH A LOW-ASPECT-RATIO UNSWEPT WING AND A TEE-TAIL*

By William H. Andrews and Herman A. Rediess

SUMMARY

A flight-test investigation of a supersonic airplane with a low-aspect-ratio unswept wing provided data in the trim angle-of-attack range for obtaining the longitudinal, lateral, and directional stability and control derivatives between Mach numbers of 0.88 and 2.08. The longitudinal-stability and three-axes control derivatives were determined by somewhat standard simplified methods, whereas the time-vector method was employed in the analysis of the lateral and directional stability derivatives.

The general correlation of the flight-determined derivatives with wind-tunnel results was good, except for a discrepancy in the absolute level of the effective dihedral derivative and the damping-in-roll derivative.

An improvement of approximately 10 to 15 percent in the static directional stability was realized in the supersonic speed range by the installation of a ventral fin on the airplane.

In the region between a Mach number of 1.38 and 1.43, an abrupt loss in the directional damping to slightly unstable conditions was experienced. At Mach numbers greater than 1.43, the damping was relatively low, but positive.

The application of the time-vector method of analysis to determine the lateral and directional derivatives was modified by incorporating the yawing velocity as a reference instead of the usual sideslip angle. This modification tended to improve the reliability and reduce the labor involved in utilizing the method.

*Title, Unclassified.

INTRODUCTION

In recent years, flight-test investigations of high-performance airplanes have been guided by utilizing analog computers as flight simulators. To simulate the response characteristics of the airplane for various flight conditions, complete information pertaining to the stability and control derivatives of the test vehicle is required. Wind-tunnel and free-flight rocket-model experiments have provided an extensive amount of derivative information on high-performance airplanes. However, experience has indicated that it is desirable to substantiate model data and theory with full-scale flight-test data, especially when full-scale phenomena cannot be duplicated by model tests.

The purpose of this paper is to present a comprehensive coverage of the stability and control derivatives of a supersonic airplane with a low-aspect-ratio unswept wing in 1 g trimmed flight. The flight-determined derivatives were calculated from data obtained in the Mach number range of 0.88 to 2.08 between the altitudes of 38,000 and 42,000 feet. These data are compared with the wind-tunnel data presented in references 1 to 9, as well as with unpublished wind-tunnel data.

In addition, the paper presents further experience in the determination of the lateral and directional stability derivatives through the application of the time-vector method of analysis and indicates a means of improving the results derived from the method by utilizing a more reliable basic reference. Reference 10 employed sideslip angle as a reference in the analysis, whereas the present investigation utilizes yawing velocity as a basic reference.

The flight-test investigation was conducted at the NASA High-Speed Flight Station at Edwards, Calif.

SYMBOLS AND COEFFICIENTS

The results of this investigation are referred to the body system of axes, inasmuch as the flight-test instrumentation is alined with these axes.

a_n normal acceleration, g units

a_t transverse acceleration, g units

b wing span, ft

C_L lift coefficient, $\frac{\text{Lift}}{\bar{q}S}$

C_{L_O} trim 1 g lift coefficient, $\frac{W}{\bar{q}S}$

C_l rolling-moment coefficient, $\frac{\text{Rolling moment}}{\bar{q}Sb}$

C_m pitching-moment coefficient, $\frac{\text{Pitching moment}}{\bar{q}S\bar{c}}$

C_n yawing-moment coefficient, $\frac{\text{Yawing moment}}{\bar{q}Sb}$

C_Y lateral-force coefficient, $\frac{\text{Lateral force}}{\bar{q}S}$

$\bar{c}$ mean aerodynamic chord, ft

g acceleration due to gravity, ft/sec^2

h_p pressure altitude, ft

I_X moment of inertia of airplane about X-axis, $slug\text{-}ft^2$

I_Y moment of inertia of airplane about Y-axis, $slug\text{-}ft^2$

I_Z moment of inertia of airplane about Z-axis, $slug\text{-}ft^2$

I_{XZ} product of inertia referred to X- and Z-axes, $slug\text{-}ft^2$

i_t stabilizer deflection, positive when trailing edge is down, deg

M Mach number

m mass of airplane, W/g, slugs

P period of damped natural frequency of airplane, sec

p rolling angular velocity, radians/sec

p' rolling angular velocity factor, $\frac{pb}{2V}$

$\dot{p}$	rolling angular acceleration, radians/sec^2
q	pitching angular velocity, radians/sec
$\dot{q}$	pitching angular acceleration, radians/sec^2
$\bar{q}$	dynamic pressure, lb/sq ft
r	yawing angular velocity, radians/sec
r'	yawing angular velocity factor, $\frac{rb}{2V}$
$\dot{r}$	yawing angular acceleration, radians/sec^2
S	wing area, sq ft
$T_{1/2}$	time required for oscillation to damp to half amplitude, sec
t	time, sec
V	free-stream velocity, ft/sec
W	weight of airplane, lb
α	angle of attack of airplane, deg or radians
β	angle of sideslip, deg or radians
δ_a	aileron deflection, positive when left aileron is deflected down, deg
δ_{a_t}	total aileron deflection, deg
δ_{yd}	yaw damper deflection, positive when deflected to left, deg
ζ	ratio of the actual damping to critical damping, $\sin \Phi_d$
τ	time parameter, $m/\rho VS$
ρ	mass density of air, slugs/cu ft
Φ	phase angle, deg

Φ_d damping angle, deg, $\tan^{-1}\frac{0.1103P}{T_{1/2}}$

$C_{L_\alpha}, C_{l_\beta}, C_{l_{\delta_a}}$
$C_{m_\alpha}, C_{m_{i_t}}, C_{n_\beta}$
$C_{n_{\delta_a}}, C_{n_{\delta_{yd}}}, C_{Y_\beta}$
} derivative of coefficient with respect to subscript

$C_{l_p}, C_{l_r}, C_{n_p}$
$C_{n_r}, C_{n_{\dot\beta}}$
} derivative of coefficient with respect to subscript $\times \frac{b}{2V}$

$C_{m_q}, C_{m_{\dot\alpha}}$ derivative of coefficient with respect to subscript $\times \frac{\bar{c}}{2V}$

The symbol $|i|$ represents the absolute magnitude of an i quantity. When employed in an equation, the equation is considered to be a vector equation.

The phase angle of a vector i relative to a reference vector k is indicated by the subscripts in Φ_{ik}.

A dot over a letter indicates the derivative with respect to time.

AIRPLANE

The test airplane is a supersonic fighter powered by a turbojet engine equipped with afterburner; a three-view drawing is shown in figure 1.

The general physical characteristics consist of a high-fineness-ratio, circular fuselage; low-aspect-ratio unswept wing; and an all-movable horizontal tail mounted near the top of the vertical tail. The wing has an airfoil thickness of 3 percent and is mounted with -10° dihedral. The vertical tail is swept 35° at the quarter chord and includes a conventional rudder and separate yaw-damper surface. After the initial flights of the airplane, a ventral fin was installed on the rear portion of the fuselage by the manufacturer to improve the directional stability.

The longitudinal and lateral controls consist of irreversible hydraulic systems. The artificial feel for the longitudinal system is provided

through a spring and bobweight combination; the lateral feel is obtained through a centering spring mechanism. Directional control is obtained through a cable-actuated rudder without the aid of power boost. A three-axes damper system was installed in the airplane; however, the damper systems were not activated during this program.

The physical characteristics of the airplane are listed in table I, and a comparison of the pertinent physical characteristics with those of the wind-tunnel models of references 1 to 9 is shown in table II. The mass and inertia characteristics are presented in figure 2. The weight ranged between approximately 16,500 and 14,000 pounds; the center of gravity ranged between approximately 14 and 8 percent mean aerodynamic chord. The values of I_X, I_Y, and I_Z were taken from the manufacturer's estimate and are referenced to the body axes. The product of inertia was calculated from these inertia values using an inclination of the principal axes of 2.9° obtained from the manufacturer.

INSTRUMENTATION

Standard NASA instruments were used to record airspeed; altitude; angle of sideslip; angle of attack; normal and transverse accelerations; pitch, roll, and yaw velocities and accelerations; and control surface deflections. The airspeed, altitude, angle of attack, and sideslip angles were sensed on a nose boom. All instruments were synchronized at 0.1-second intervals by a common timer.

The turnmeters used to measure the angular velocities and accelerations were referenced to the airplane body axes and were mounted within 0.2° of these axes.

The ranges, scales of the recorded data, and dynamic characteristics for angle-of-attack, sideslip, velocity, and acceleration instruments are:

Function	Range	Scale of recorded data (per in. deflection)	Undamped natural frequency, cps	Damping ratio
α, deg	-23 to 34	10.40	10.5	0.65
β, deg	±30	10.50	10.5	.65
p, radians	±2	2.20	19.0	.68
q, radians	±.28	.29	6.5	.61
r, radians	±.10	.09	6.5	.66
a_n, g	-1 to 8	5.14	32.0	.67
a_t, g	±.5	.56	18.6	.65

Indicated sideslip angles and angles of attack measured by vane-type pickups were corrected for roll and yaw rate effects and pitch rate effects, respectively. The pickups were mass damped and had dynamically flat frequency-response characteristics over the frequency range of the airplane.

All data employed in the analysis were corrected for instrument phase lag. Position corrections were applied to indicated linear accelerometer readings by the time-vector method (ref. 10).

TESTS

The general procedure employed to obtain data during this investigation was to measure the airplane response to an abrupt control deflection at specified altitude and Mach number conditions. So that the applied methods of analysis would yield the best results, considerable emphasis was placed on maintaining constant altitude and Mach number, and control-fixed conditions during the transient phase of the maneuvers.

The tests were conducted over the Mach number range from 0.88 to 2.08 at an altitude of 40,000 feet, with a deviation of ±2,000 feet during the program. All data were obtained at the 1.0g (±0.1g) trim conditions presented in figure 3.

The longitudinal data were obtained from abrupt triangular-shaped stabilizer pulses ranging between -2° and -3° deflection. The lateral and directional data were resolved from the abrupt aileron or pilot-activated yaw-damper input of rectangular shape. The aileron deflections ranged from 25 percent to full deflection. The yaw-damper data presented are for full deflection of the damper surface. During a particular maneuver only the control necessary to produce the primary airplane disturbance was deflected; all other control surfaces were maintained in the fixed trim position.

ANALYSIS AND DATA PRESENTATION

Longitudinal

The flight records, typified by the time histories of figure 4, were reduced to the basic values of P, $T_{1/2}$, ζ, and amplitude ratio $\frac{|a_n|}{|\alpha|}$ presented in figure 5. To determine the derivatives C_{L_α}, C_{m_α},

and $\left(C_{m_q} + C_{m_{\dot{\alpha}}}\right)$ of figure 6, the basic data were substituted in the following simplified expressions:

$$C_{L_\alpha} = C_{L_0}\frac{|a_n|}{|\alpha|}$$

$$C_{m_\alpha} = \frac{-I_Y}{\bar{q}S\bar{c}}\left[\left(\frac{2\pi}{P}\right)^2 + \left(\frac{0.693}{T_{1/2}}\right)^2\right]$$

and

$$\left(C_{m_q} + C_{m_{\dot{\alpha}}}\right) = \frac{4VI_Y}{\bar{q}S\bar{c}^2}\left(\frac{C_{L_\alpha}}{4\tau} - \frac{0.693}{T_{1/2}}\right)$$

The control effectiveness $C_{m_{i_t}}$ (fig. 6) was calculated from data obtained during the initial stabilizer input portion of the time history. The peak acceleration and corresponding incremental velocity were substituted in the following relation to obtain this parameter:

$$C_{m_{i_t}} = \frac{1}{\Delta i_t}\left[\frac{I_Y}{\bar{q}S\bar{c}}\Delta\dot{q} - \frac{\bar{c}}{2V}\left(C_{m_q} + C_{m_{\dot{\alpha}}}\right)\Delta q\right]$$

The flight-determined derivatives and the wind-tunnel data used for comparison (fig. 7) were corrected to a center-of-gravity location of 10 percent mean aerodynamic chord.

Lateral and Directional

The static and dynamic stability derivatives C_{n_β}, $\left(C_{n_r} - C_{n_{\dot{\beta}}}\right)$, C_{l_β}, C_{l_p}, and C_{Y_β} were determined by the time-vector method. The application of the method utilizes transient response time-history data from yaw-damper pulses similar to those included in figure 8. From these data, the pertinent quantities of period, damping, amplitude ratio, and phase angles were determined and are summarized in figures 9 to 11.

Reference 10 includes an extensive discussion of the time-vector method and its limitations. In the present analysis, the results are referenced to the body axes instead of the stability axes system, and

the amplitude ratios and phase angles are measured with respect to the yawing velocity. By using the yawing velocity as a basic reference, it was possible to complete the analysis without relying on the measured sideslip angles, as was done in references 10 and 11. When the sideslip angle is employed as a reference, difficulties arise which require an iterative process in the initial phase of the analysis. With the yaw velocity as a reference this iteration is eliminated, and the consistency and reliability of the results are believed to be improved.

The equations of motion and representative time-vector diagrams are shown in figure 12. In the vector solution of the yaw and roll equations values of C_{n_p} were obtained from an estimate by the manufacturer, and values of C_{l_r} were assumed on the basis of unpublished wind-tunnel data. Figures 13 and 14 show the flight-determined derivatives.

The aileron and yaw-damper control-effectiveness derivatives (fig. 15) were obtained by a method similar to that employed in the determination of the longitudinal control effectiveness. The incremental rolling and yawing velocities and corresponding peak accelerations associated with the control input during aileron pulses and rolls were substituted into the following simplified equations to obtain the aileron effectiveness:

$$C_{l_{\delta_a}} = \frac{1}{\Delta\delta_a}\left(\frac{I_X}{\bar{q}Sb}\Delta\dot{p} - \frac{I_{XZ}}{\bar{q}Sb}\Delta\dot{r} - \frac{b}{2V}C_{l_p}\Delta p\right)$$

and

$$C_{n_{\delta_a}} = \frac{1}{\Delta\delta_a}\left[\frac{I_Z}{\bar{q}Sb}\Delta\dot{r} - \frac{I_{XZ}}{\bar{q}Sb}\Delta\dot{p} - \frac{b}{2V}\left(C_{n_r} - C_{n_{\dot{\beta}}}\right)\Delta r\right]$$

Yaw-damper effectiveness was derived from the substitution of the yaw velocities and accelerations in the expression:

$$C_{n_{\delta_{yd}}} = \frac{1}{\Delta\delta_{yd}}\left[\frac{I_Z}{\bar{q}Sb}\Delta\dot{r} - \frac{b}{2V}\left(C_{n_r} - C_{n_{\dot{\beta}}}\right)\Delta r\right]$$

In the comparison of the flight-determined derivatives with wind-tunnel results (figs. 16 to 18) an attempt was made to calculate the wing flexibility corrections to the wind-tunnel values of C_{l_β} and C_{l_p} by the method outlined in appendix B of reference 11. The calculations revealed that the influence was insignificant for the motion excursions

experienced by the airplane during the investigation. The wind-tunnel values of C_{n_β} and C_{Y_β} have been corrected for the effects of vertical-tail flexibility by the method of reference 12 and by utilizing the manufacturer's estimated effects of flexibility on vertical-tail effectiveness. The value of ΔC_{n_β} due to flexibility varied between approximately 0.0003 to 0.0008 per deg over a Mach number range from 0.90 to 2.01. The influence of the incremental side force at the engine inlet resulting from the momentum change caused by turning the intake air into the inlet duct was found to be negligible.

Analog Simulation

In addition to the preceding analysis, an analog investigation was conducted to assess the validity of the derivatives. A simulation of the flight time history was obtained on a five-degree-of-freedom analog setup. The control input was programmed into the machine through a plotting table, and the resulting airplane responses were compared with an overlay of the flight records. During the investigation, the flight-determined derivatives were adjusted to the values indicated by the solid symbols of figures 6, 13, and 15 in order to match the time histories of figures 4 and 8.

DISCUSSION

Longitudinal Stability

Basic data.- The period, damping ratio, and amplitude ratio data of figure 5 indicate no unusual deviations. In the transonic range, the period and damping ratio exhibit rapid changes and a degree of scatter which are usually associated with the aerodynamic behavior in this region. The extent of this behavior, discussed in reference 13, is a function of such factors as wing thickness, aspect ratio, and taper ratio.

The period and damping ratios vary from 2.3 to 1.1 and 0.17 to 0.90, respectively, over the speed range. Above $M \approx 1.7$ these quantities increase over the minimum values mentioned.

Flight derivatives.- The general trends of the stability and control derivatives (fig. 6) over the Mach number range appear uniform, with the exception of C_{m_α} and $\left(C_{m_q} + C_{m_{\dot{\alpha}}}\right)$. In the transonic region C_{m_α}

indicates the expected rapid increase between $M = 0.89$ and 0.92. The damping derivative $\left(C_{m_q} + C_{m_{\dot{\alpha}}}\right)$ exhibits a gradual, but significant, decrease between $M = 1.05$ and 1.25.

By observing the solid symbols of figure 6, it is evident that only minor adjustments to the flight-determined derivatives were required to obtain the analog simulation of the flight time histories of figure 4.

Wind-tunnel comparison.- The general correlation between the wind-tunnel and flight-determined derivatives of figure 7 is good, especially in the transonic region. The abrupt increase in C_{m_α} previously mentioned appears to be well confirmed by the existing wind-tunnel data in this region. The values of C_{m_α} from reference 1 show an appreciable deviation from the trend of the flight results at Mach numbers of 1.35 and 1.45. The reason for this discrepancy is not readily apparent, inasmuch as the same source of comparison shows good agreement at the higher speeds.

Lateral and Directional Stability

Basic data.- The period of the transient oscillation shown in figure 9 remains fairly constant at a value of approximately 1.6 seconds over the supersonic speed range, although a definite loss in damping is indicated between $M = 1.38$ and 1.43. Beyond $M = 1.43$ the damping increases slightly, but still remains near zero.

An attempt was made to associate the abrupt loss in damping with the shock-wave interaction from various components of the airplane. Although a cursory analysis indicated that shocks emanating from the wing trailing edge in this speed range would probably impinge on the vertical tail, the shock system can be so complex (ref. 14) that relating the loss in damping to any one shock system or phasing of any particular system becomes mere speculation. It is believed, however, that the interference from various shock-wave patterns may be the cause of this phenomenon.

The variations of amplitude ratio and phase angles of figures 10 and 11 show no unusual trends except in the region, mentioned previously, between $M = 1.38$ and 1.43. The amplitude ratios of $\frac{|a_t|}{|r|}$ and $\frac{|\beta|}{|r|}$ range from 2 to 4 and 0.5 to 0.3, respectively. The ratio of $\frac{|p|}{|r|}$ varies between 8 and 5.5, which is somewhat higher than that indicated by several comparable research airplanes.

The degree of scatter exhibited by the amplitude ratio and phase angle data is a minimum, with the exception of the roll-to-yaw phase angle Φ_{pr} which shows a maximum deviation from the mean of approximately $\pm 7^{\circ}$. This deviation occurs primarily in the transonic region where the Mach number is difficult to control during the transient phase of a test maneuver. The consistency of the $\frac{|\beta|}{|r|}$ and $\Phi_{\beta r}$ is attributed to the fact that these quantities were calculated from the transverse acceleration equation. It was possible to obtain these quantities in this manner, rather than by relying on direct measurements, inasmuch as the yawing velocity was employed for the basic reference, as discussed in detail in the analysis section.

Flight derivatives.- The variation of the static-stability derivatives with Mach number presented in figure 13 exhibits good consistency. However, in the evident scatter of the results it is believed that the data between $M = 1.38$ and 1.43 indicate a possible shock-wave effect.

From an observation of the limited flight-determined C_{n_β} data obtained without the ventral fin, it appears that an extrapolation of the results to the higher speeds would agree favorably with the manufacturer's flight results (see fig. 13). It is evident that incorporation of the ventral fin on the airplane increased C_{n_β} by approximately 10 to 15 percent over the supersonic speed range. The general trend of the variations of C_{n_β} and C_{l_β} with Mach number for the configuration with the ventral fin installed indicates approximately a 60- to 65-percent reduction in these parameters over the speed range tested.

The damping-in-yaw derivative $\left(C_{n_r} - C_{n_{\dot{\beta}}}\right)$ remains fairly constant at -1 over the speed range to $M = 2.08$ (fig. 14). However, in the region between $M = 1.38$ and 1.43 where the abrupt loss in damping occurs (fig. 9), $\left(C_{n_r} - C_{n_{\dot{\beta}}}\right)$ increases to -2, then abruptly drops to -0.2 or 0. The amount of scatter over the speed range is insignificant except in the transonic region.

The damping-in-roll derivative C_{l_p} varies from -0.6 to -0.28 between $M = 0.95$ and 2.08, and an abrupt decrease from -0.57 to -0.42 occurs between $M = 1.38$ and $M = 1.47$.

Although the derivatives C_{l_β} and C_{l_p} were derived from the same vector diagram, the variation of C_{l_β} with Mach number appears more consistent than the variation of C_{l_p}. A study of the orientation of

the vectors representing C_{l_β} and C_{l_p} in the roll equation (fig. 12) indicates that a deviation of the phase angle Φ_{pr} will have a greater influence on the magnitude of C_{l_p} than on C_{l_β}. Consequently, the previously mentioned scatter in Φ_{pr} is reflected in the results of C_{l_p}.

The aileron effectiveness $C_{l_{\delta_a}}$ and cross-control derivative $C_{n_{\delta_a}}$ (fig. 15) indicate a nonlinear moment variation with aileron deflection up to $M \approx 1.4$; however, this is more evident at $M < 1$. Over the test Mach number range the control effectiveness decreases about 75 to 80 percent. The $C_{n_{\delta_a}}$ is an appreciable positive value in the transonic region and decreases to approximately zero with increasing Mach number. The yaw-damper effectiveness $C_{n_{\delta_{yd}}}$ indicates a loss of 75 percent between $M = 0.95$ and 2.08.

The solid symbols of figures 13 to 15 represent the values of the derivatives employed in the analog simulation of the time histories of figure 8. With the exception of C_{l_β} at $M = 1.25$, it can be seen that only minor adjustments of the flight-determined derivatives were required to obtain good simulation results. The reason for the discrepancy in C_{l_β} at $M = 1.25$ was not apparent.

Wind-tunnel comparison.- Generally, the agreement between the wind-tunnel and flight-determined C_{n_β} is good (fig. 16). The ventral-on data at $M = 1.8$ and 2.0 from the Ames 9 × 7 foot Unitary Plan wind tunnel are superimposed on the flight data. The incremental value from ventral-on to ventral-off of 0.0008 per degree is approximately the same for the wind-tunnel results as for the flight results in the high-speed range (see figs. 13 and 16).

Comparison of the flight-determined roll derivatives C_{l_β} and C_{l_p} with wind-tunnel results (figs. 16 and 17) indicates that the flight data were consistently high over the entire speed range. It was concluded, after considering several possible sources of error in the analysis, that an error could have been made in the estimated moment of inertia I_X. Consequently, the flight data were recalculated assuming a 20-percent reduction in I_X, and the results show a somewhat better comparison with the wind-tunnel data. This does not imply conclusively that the estimated inertias or the associated derivatives were incorrect, but it does appear to be a possible explanation for the discrepancy shown.

The correlation of the unpublished wind-tunnel values of $\left(C_{n_r} - C_{n_{\dot{\beta}}}\right)$ of figure 17 with the flight-determined results, which were calculated using the manufacturer's estimate of C_{n_p}, shows good agreement. After the analysis had been completed, unpublished wind-tunnel data became available which included a variation of C_{n_p} with Mach number (fig. 17). These data were incorporated in a recalculation of C_{n_β} and $\left(C_{n_r} - C_{n_{\dot{\beta}}}\right)$, and the results are presented in figures 16 and 17, respectively. It can be seen that the primary deviation from the originally computed C_{n_β} and $\left(C_{n_r} - C_{n_{\dot{\beta}}}\right)$ occurs in the region between $M = 0.95$ and 1.5. The values of C_{n_β} do not change appreciably; however, the recalculated values of $\left(C_{n_r} - C_{n_{\dot{\beta}}}\right)$ show poor correlation with the wind-tunnel results in this region.

The comparison of the control parameters of figure 18 shows good agreement between the flight-determined and wind-tunnel results, except for the values of $C_{n_{\delta_a}}$.

CONCLUSIONS

Results of a flight-test investigation to determine the stability and control derivatives of a supersonic airplane, with a low-aspect-ratio unswept wing, between a Mach number of 0.88 and 2.08 in the low angle-of-attack range led to the following conclusions.

1. The longitudinal damping is relatively constant; however, the longitudinal stability derivative C_{m_α} exhibits an abrupt increase between a Mach number of 0.88 and 0.92, then gradually decreases with further increase in supersonic Mach number.

2. The directional stability derivative C_{n_β} and the effective dihedral derivative C_{l_β} decrease approximately 60 to 65 percent between a Mach number of 0.88 and 2.08.

3. Installation of a ventral fin on the airplane improved the directional stability by 10 to 15 percent at supersonic speeds.

4. An abrupt loss in the directional damping was indicated in the region between a Mach number of 1.38 and 1.43. At Mach numbers greater than 1.43, the damping was relatively low, but positive.

5. The aileron effectiveness derivative $C_{l_{\delta_a}}$ was reduced by approximately 75 to 80 percent over the test range and indicated an appreciable nonlinear variation of rolling moment with aileron deflection at Mach numbers less than 1.

6. The general agreement between the flight-determined derivatives and the wind-tunnel results is good, with the exception of a discrepancy in the absolute level of the effective dihedral derivative and the damping-in-roll derivative.

7. The incorporation of the yawing velocity as a reference instead of the usual sideslip angle in the time-vector analysis showed a tendency to improve the data reliability and reduced the labor involved in the application of the method.

High-Speed Flight Station,
National Aeronautics and Space Administration,
Edwards, Calif., October 29, 1958.

REFERENCES

1. Smith, Willard G.: Wind-Tunnel Investigation at Subsonic and Supersonic Speeds of a Fighter Model Employing a Low-Aspect-Ratio Unswept Wing and a Horizontal Tail Mounted Well Above the Wing Plane - Longitudinal Stability and Control. NACA RM A54D05, 1954.

2. Hieser, Gerald, and Reid, Charles F., Jr.: Transonic Longitudinal Aerodynamic Characteristics of a Fighter-Type Airplane Model With a Low-Aspect-Ratio Unswept Wing and a Tee-Tail. NACA RM L54K19a, 1956.

3. Robinson, Ross B.: Longitudinal Characteristics of an Unswept-Wing Fighter-Type Model With External Stores at a Mach Number of 1.82 and Some Effects of Horizontal-Tail and Yaw-Damper-Vane Deflection on the Sideslip Derivatives. NACA RM L55L26, 1956.

4. Spearman, M. Leroy, and Driver, Cornelius: Longitudinal and Lateral Stability Characteristics of a Low-Aspect-Ratio Unswept-Wing Airplane Model at Mach Numbers of 1.82 and 2.01. NACA RM L56H06, 1957.

5. Buell, Donald A., Reed, Verlin D., and Lopez, Armando E.: The Static and Dynamic-Rotary Stability Derivatives at Subsonic Speeds of an Airplane Model With an Unswept Wing and a High Horizontal Tail. NACA RM A56I04, 1956.

6. Tinling, Bruce E.: Subsonic Aerodynamic Characteristics Up to Extreme Angles of Attack of an Airplane Model Having an Unswept Wing and a High Horizontal Tail. NACA RM A57K05, 1958.

7. Sleeman, William C., Jr., and Wiggins, James W.: Experimental Investigation at High Subsonic Speeds of the Rolling Stability Derivatives of a Complete Model With an Aspect-Ratio-2.52 Wing Having an Unswept 72-Percent-Chord Line and a High Horizontal Tail. NACA RM L54I20, 1955.

8. Arabian, Donald D., and Schmeer, James W.: Lateral Stability and Control Measurements of a Fighter-Type Airplane With a Low-Aspect-Ratio Unswept Wing and a Tee-Tail. NACA RM L55F08, 1956.

9. Smith, Willard G., and Intrieri, Peter F.: Some Effects of Aileron Deflection on the Static Lateral and Directional Aerodynamic Characteristics of Four Contemporary Airplane Models. NACA RM A57E22, 1957.

10. Wolowicz, Chester H.: Time-Vector Determined Lateral Derivatives of a Swept-Wing Fighter-Type Airplane With Three Different Vertical Tails at Mach Numbers Between 0.70 and 1.48. NACA RM H56C20, 1956.

11. Gillis, Clarence L., and Chapman, Rowe, Jr.: Effect of Wing Height and Dihedral on the Lateral Stability Characteristics at Low Lift of a 45° Swept-Wing Airplane Configuration as Obtained from Time-Vector Analyses of Rocket-Propelled-Model Flights at Mach Numbers from 0.7 to 1.3. NACA RM L56E17, 1956.

12. Letko, William, and Riley, Donald R.: Effect of an Unswept Wing on the Contribution of Unswept-Tail Configurations to the Low-Speed Static- and Rolling-Stability Derivatives of a Midwing Airplane Model. NACA TN 2175, 1950.

13. Harris, William G.: A Wind-Tunnel Investigation at High-Subsonic and Low Supersonic Mach Numbers on a Series of Wings With Various Sweepback, Taper, Aspect Ratio, and Thickness. Part 2. Comparison of Lift and Stability Data. AF Tech. Rep. No. 6669. Part 2, Wright Air Dev. Center, Dec. 1952.

14. Nielsen, Jack N., and Kaattari, George E.: The Effects of Vortex and Shock-Expansion Fields on Pitch and Yaw Instabilities of Supersonic Airplanes. Preprint No. 743, Inst. Aero. Sci., June 1957.

TABLE I.- GEOMETRIC CHARACTERISTICS OF THE AIRPLANE

Wing:	
Airfoil section	Modified biconvex
Area, sq ft	196.1
Span, ft	21.94
Mean aerodynamic chord, ft	9.55
Root chord, ft	12.98
Tip chord, ft	4.89
Aspect ratio	2.45
Taper ratio	0.378
Sweep at 25 percent chord, deg	18.1
Sweep at the leading edge, deg	27.3
Incidence, deg	0
Dihedral, deg	-10.0
Airfoil thickness ratio	0.0336
Leading-edge flaps (per side) -	
Area, sq ft	8.50
Mean chord, ft	1.012
Deflection limit, deg	-30.0
Type	Plain
Trailing-edge flaps (per side) -	
Area, sq ft	11.55
Mean chord, ft	2.52
Deflection limit, deg	45.0
Type	Plain
Ailerons (per side) -	
Area, sq ft	4.73
Mean chord, ft	1.716
Span, ft	2.75
Deflection	±15.0
Tail:	
Horizontal tail -	
Airfoil section	Modified biconvex
Area, sq ft	48.2
Mean aerodynamic chord, ft	4.415
Span, ft	11.92
Root chord, ft	6.16
Tip chord, ft	1.917
Aspect ratio	2.95
Taper ratio	0.311
Root thickness ratio	0.0493
Tip thickness ratio	0.0261
Tail length, 0.25 wing mean aerodynamic chord to 0.25 horizontal-tail mean aerodynamic chord, ft	18.72
Sweep at 0.25 mean aerodynamic chord, deg	10.12
Deflection limits, deg	5.0 to -17.0

TABLE I.- GEOMETRIC CHARACTERISTICS OF THE AIRPLANE - Concluded

Vertical tail -	
Airfoil section	Modified biconvex
Area, sq ft	35.1
Span, ft	5.46
Mean aerodynamic chord, ft	6.88
Aspect ratio	0.849
Taper ratio	0.371
Tail length, 0.25 wing mean aerodynamic chord to 0.25 vertical-tail mean aerodynamic chord, ft	15.13
Sweep at 0.25 mean aerodynamic chord, deg	35.0
Rudder -	
Area, sq ft	4.3
Span, ft	2.92
Average chord, ft	1.375
Deflection limits	±25
Yaw damper -	
Area, sq ft	1.0
Span, ft	1.0
Average chord, ft	1.0
Deflection limits, deg	±20
Fuselage:	
Frontal area, sq ft	25.0
Length, ft	51.25
Fineness ratio	9.09
Dive brakes (per side):	
Area, sq ft (projected frontal area at maximum deflection)	4.13
Chord, ft	2.50
Deflection limit	60.0
Weight:	
Empty weight, lb	13,237
Total take-off weight, lb	18,233
Center-of-gravity-location, percent mean aerodynamic chord	
Empty	17.40
Takeoff	5.25

Note: For inertia characteristics see figure 2.

TABLE II.- COMPARISON OF PHYSICAL CHARACTERISTICS OF

WIND-TUNNEL MODELS WITH FULL-SCALE AIRPLANE

References	1	2	3	4	5	6	7	8	9	Test airplane
Model scale	0.086	0.086	0.085	0.040	0.099	0.040	0.086	0.086	0.086	1.00
Wing:										
Area, sq ft	190	190	195	196	194	196	191	190	191	196.1
Span, ft	22	22	22	22	22	22	22	22	22	21.94
Aspect ratio	2.5	2.5	2.45	2.45	2.44	2.45	2.5	2.5	2.5	2.45
Mean aerodynamic chord, ft	9.3	9.3	9.4	9.5	9.5	9.5	9.3	9.3	9.3	9.55
Sweep at 25 percent chord, deg	19	18.5	18.5	18.1	19	18.2	19.1	18.5	19	18.1
Dihedral, deg	-5	-10	-10	-10	-10	-10	-10	-10	-5	-10
Taper ratio	0.385	0.385	0.377	0.377	0.38	0.38	0.384	0.385	0.384	0.378
Horizontal tail:										
Area, sq ft	47	48	49	48	48.9	48	48	48	47	48.2
Mean aerodynamic chord, ft	4.4	4.4	4.45	4.4	4.45	4.4	4.3	4.4	4.4	4.42
Span, ft	11.6	12.0	12.1	11.9	12.1	11.9	11.9	12.0	11.6	11.9
Aspect ratio	2.89	2.97	2.96	2.95	2.97	2.95	2.98	2.97	2.89	2.95
Taper ratio	0.326	0.311	0.312	0.311	0.31	0.31	0.319	0.312	0.326	0.311
Sweep at 25 percent chord, deg	10	10	10.3	10.1	10	10.1	10	10	10	10.12
Tail length, ft (0.25 wing mean aerodynamic chord to 0.25 horizontal-tail mean aerodynamic chord)	16.7	16.7	16.9	18.3	16.8	18.0	16.7	16.7	16.7	18.7
Vertical tail:										
Area, sq ft	37	34	31	36	30	35	29	34	37	35.1
Mean aerodynamic chord, ft	7	6.9	7.0	7.16	8.7	7.16	6.9	6.9	7	6.88
Aspect ratio	1.1	0.82	0.997	0.85	0.86	0.87	0.78	0.82	1.1	0.849
Taper ratio	0.38	0.4	0.463	0.378	0.37	0.46	0.462	0.4	0.38	0.371
Sweep at 25 percent chord, deg	30	35	34.77	34.9	35	35	30	35	30	35
Tail length, ft (0.25 wing mean aerodynamic chord to 0.25 vertical-tail mean aerodynamic chord)	13	13	13.3	14.9	13.5	14.9	13	13	13	15.1
Vertical height (fuselage center line to vertical-tail tip)	8.5	7.9	7.6	8.7	7.4	8.6	7.4	7.9	8.5	8.7
Ventral on	No	No	No	Yes	No	No	No	No	No	Yes

Note: Model characteristics converted to full-scale.

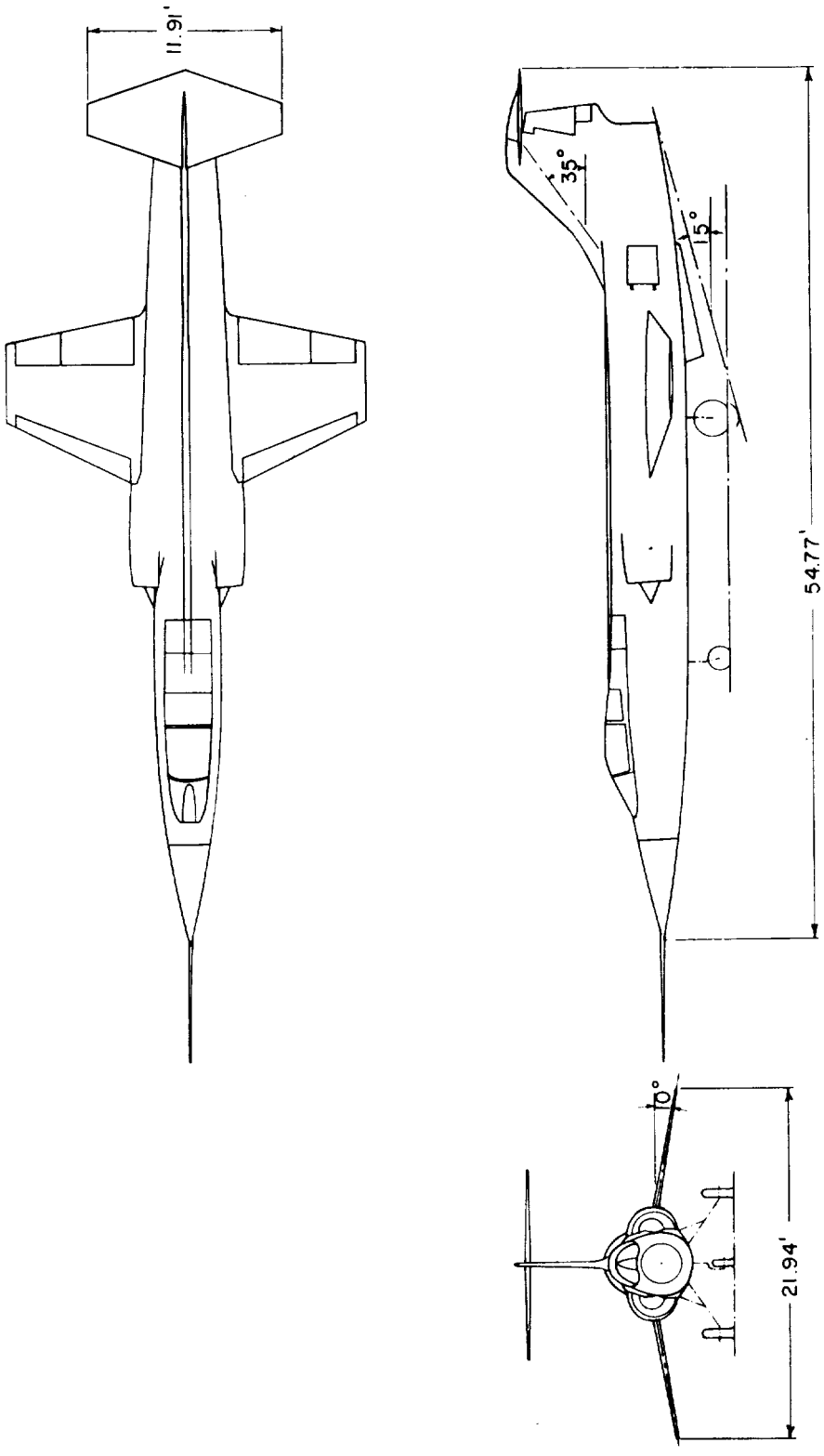

Figure 1.- Three-view drawing of the test airplane.

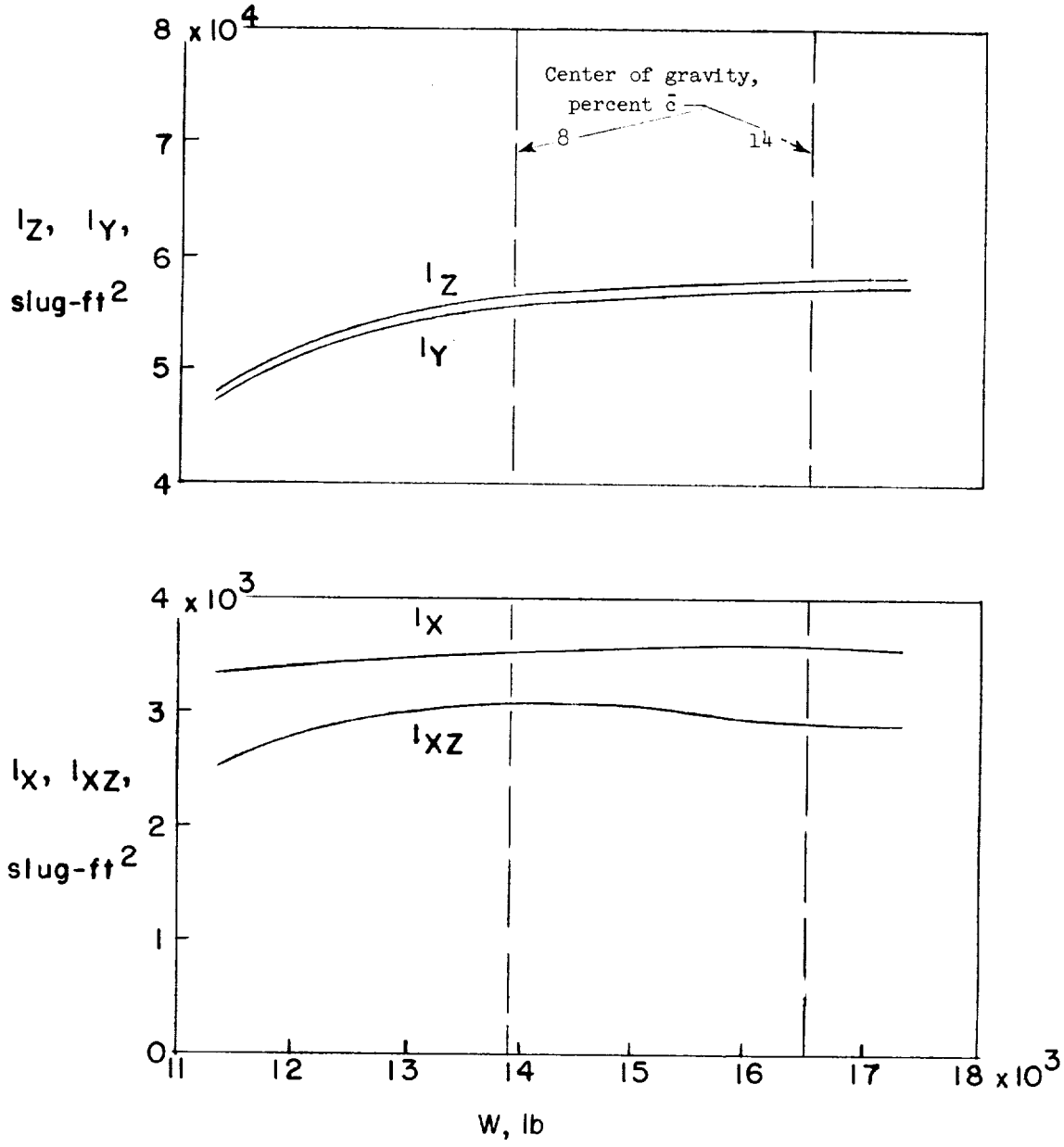

Figure 2.- Inertia characteristics of the test airplane as a function of airplane weight.

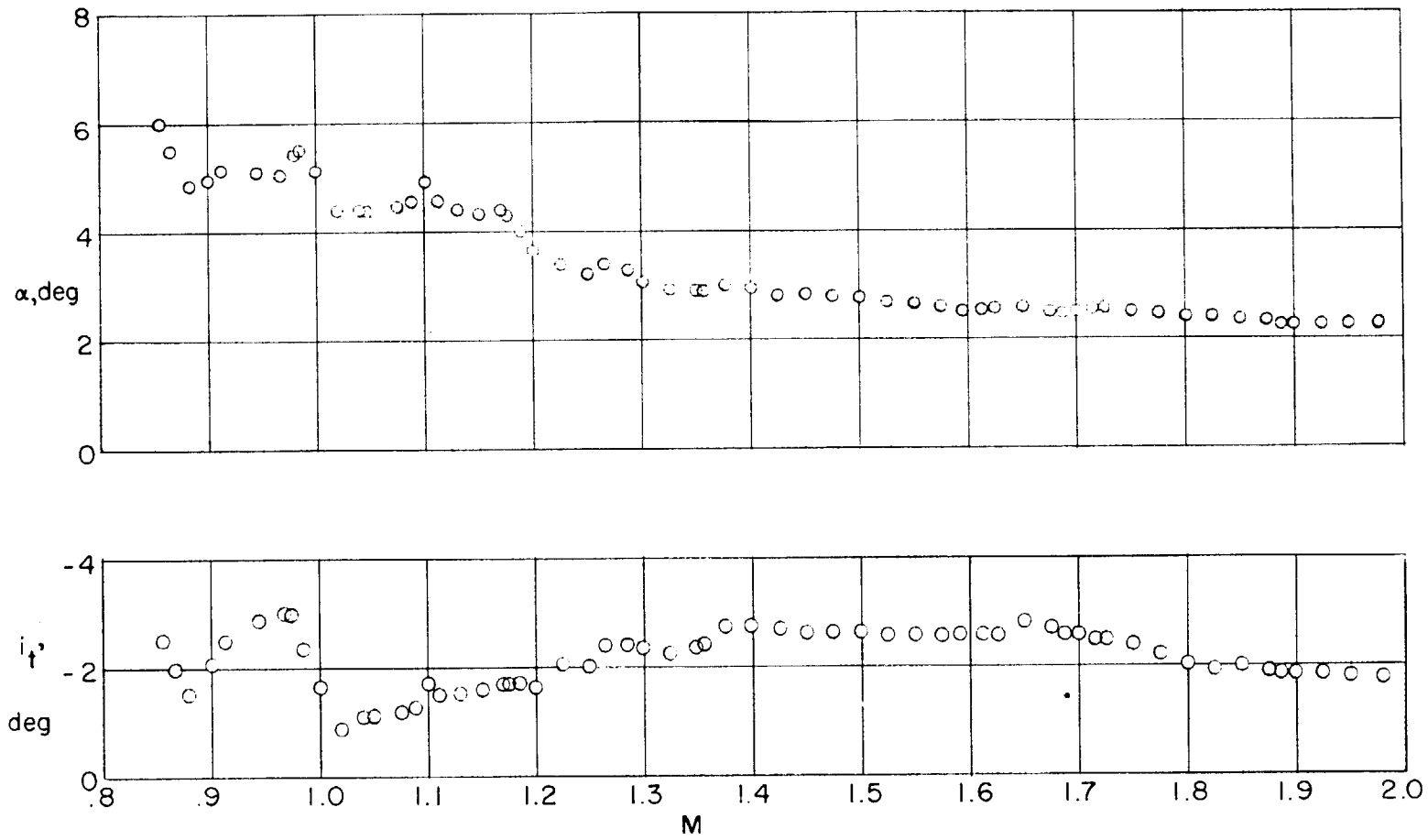

Figure 3.- Variation of the 1 g trim angle of attack and stabilizer deflection with Mach number. $h_p \approx 40{,}000$ ft.

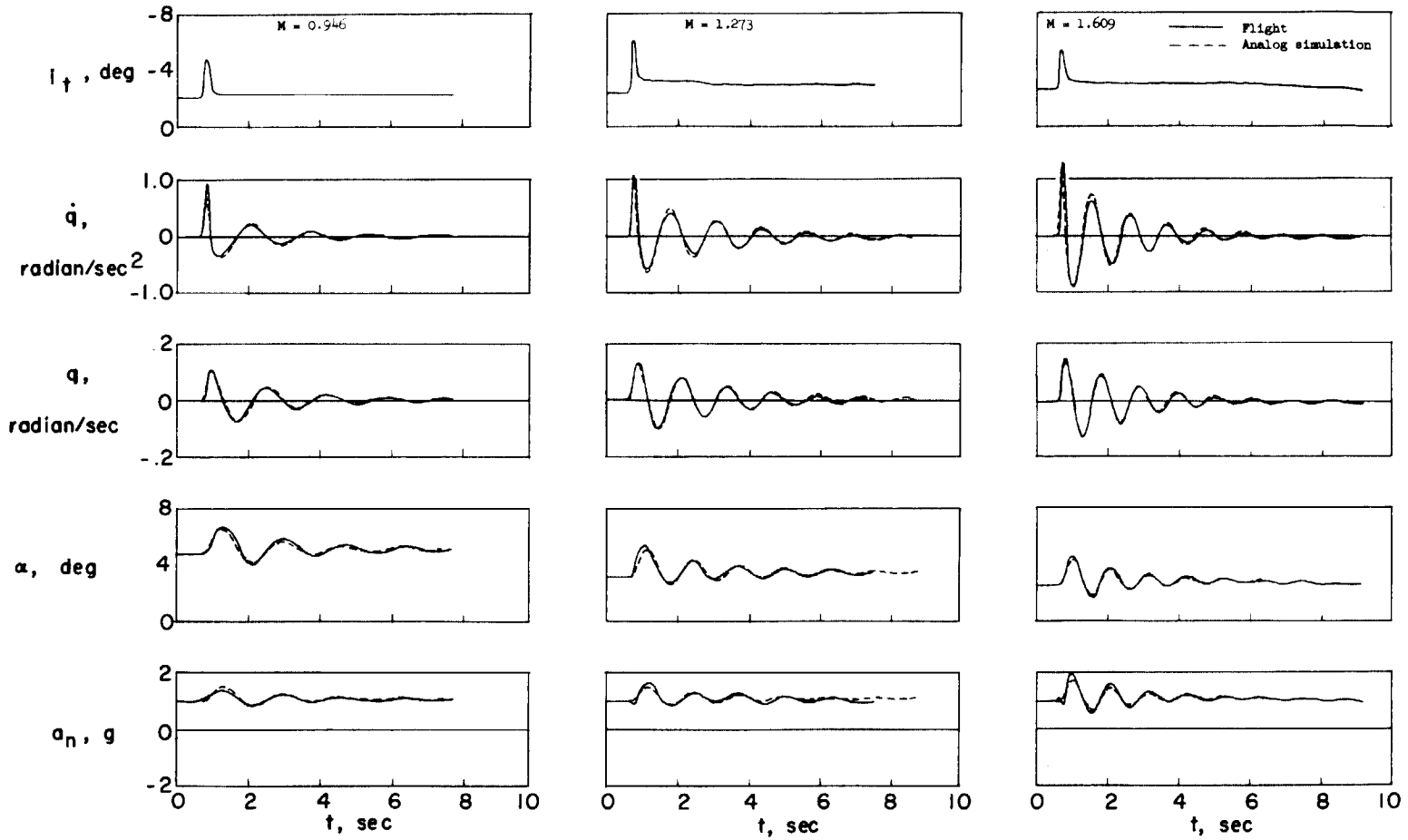

Figure 4.- Typical time histories of the longitudinal response characteristics of the test airplane resulting from abrupt stabilizer deflection.

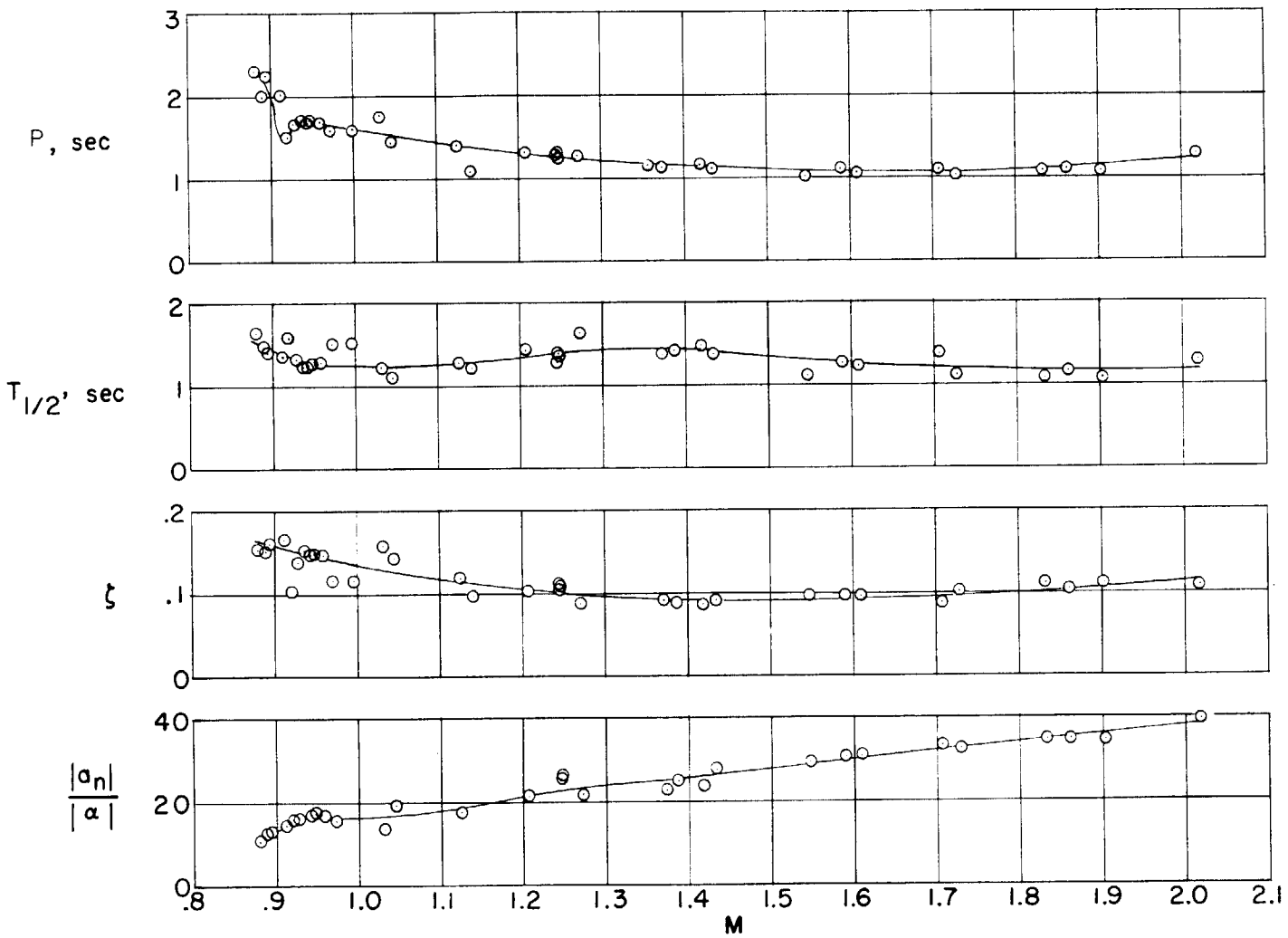

Figure 5.- Variation of the longitudinal transient-response characteristics with Mach number.

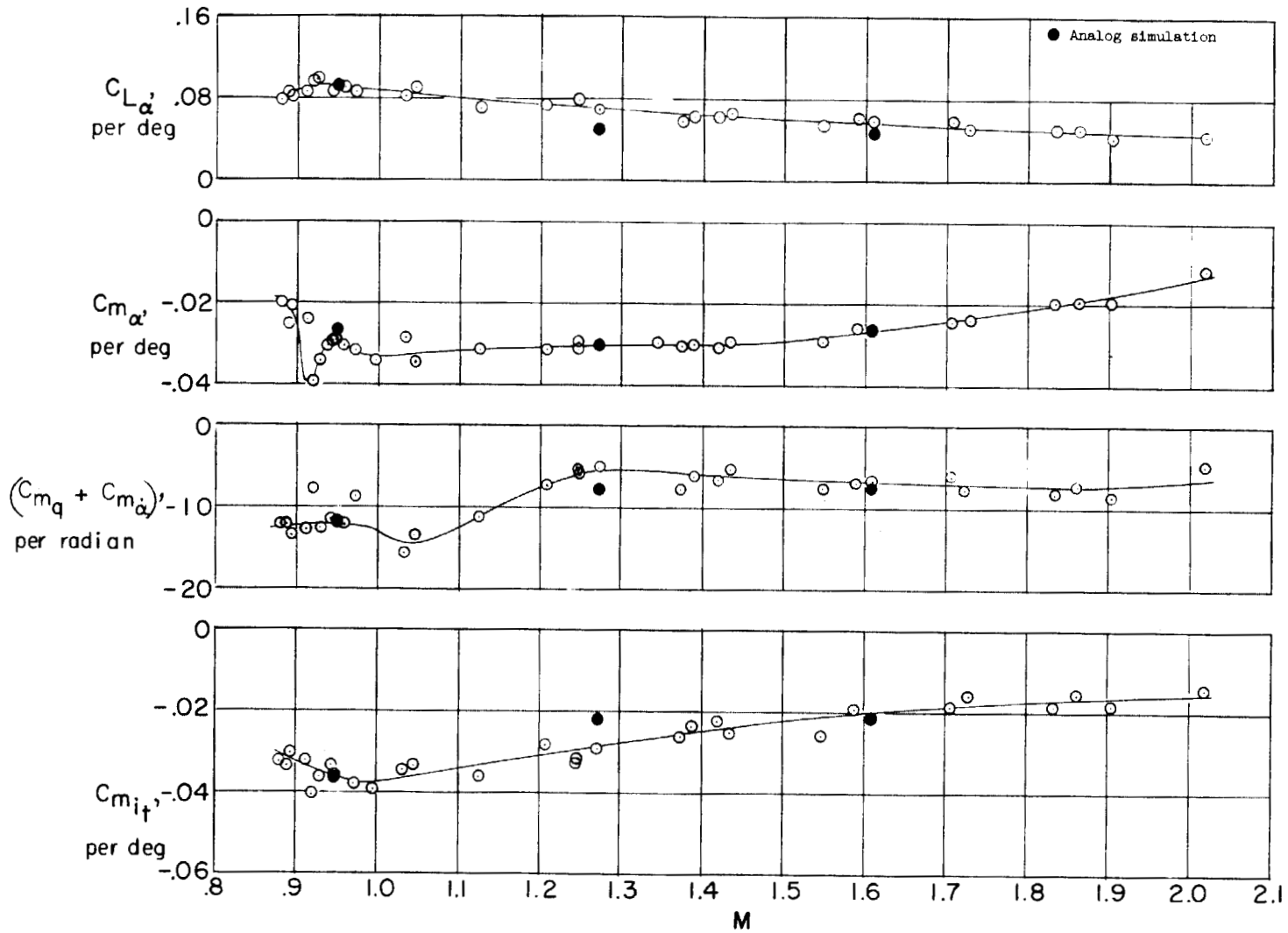

Figure 6.- Variation of the flight-determined longitudinal stability and control derivatives with Mach number.

CONFIDENTIAL

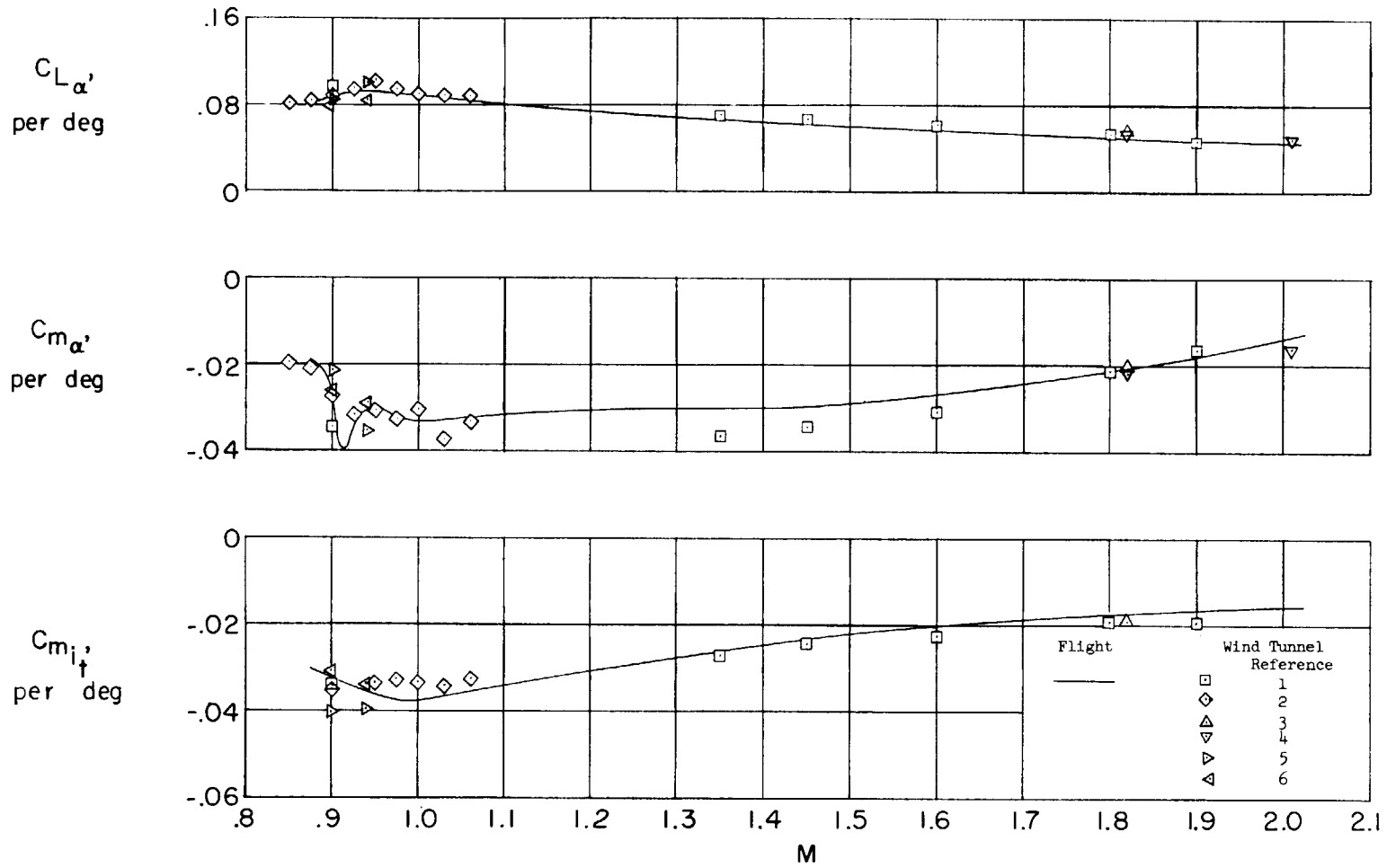

Figure 7.- Comparison of the flight-determined longitudinal stability and control derivatives with wind-tunnel results.

CONFIDENTIAL

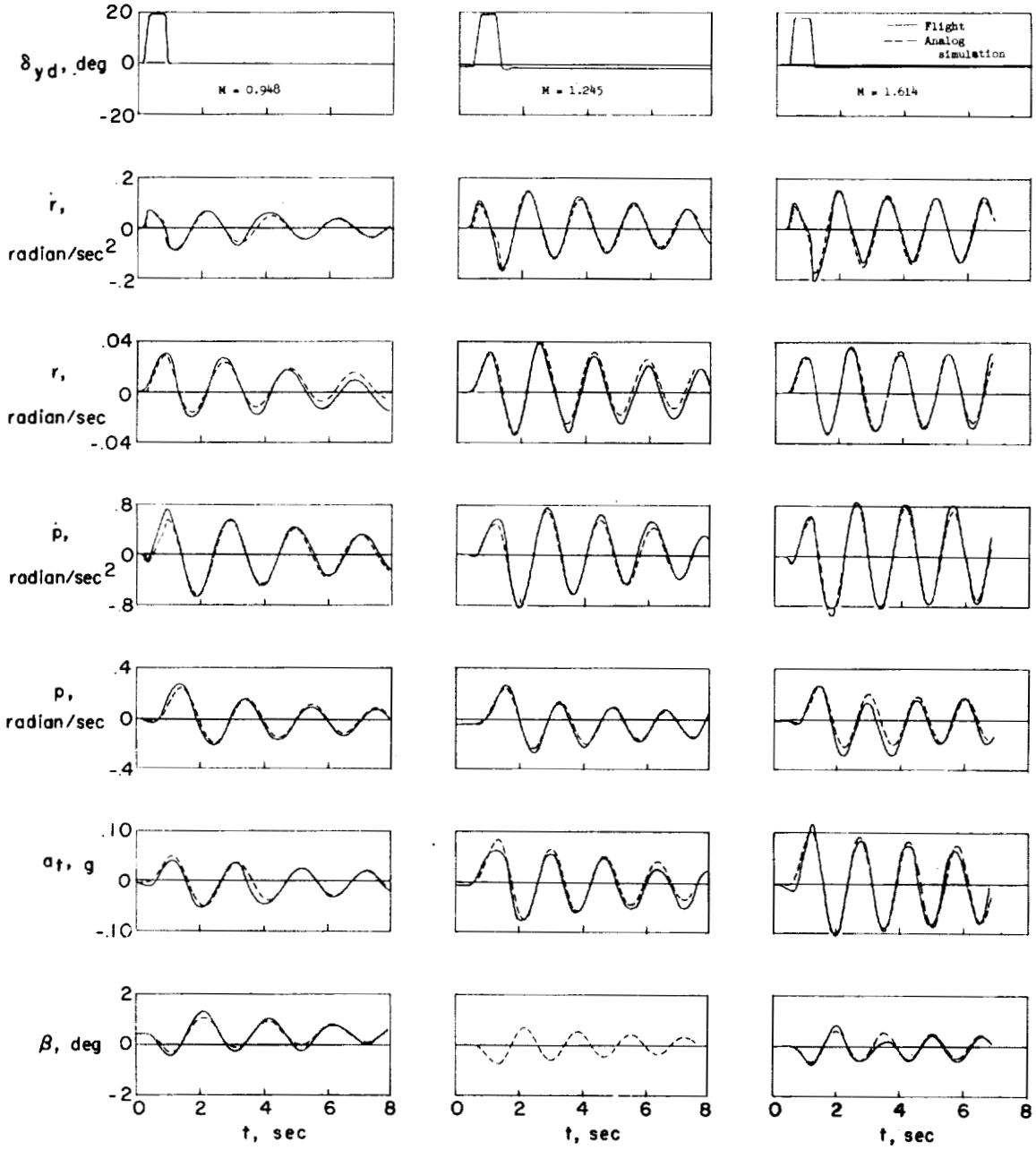

(a) Yaw-damper deflection.

Figure 8.- Typical time histories of the lateral and directional response characteristics of the test airplane resulting from abrupt yaw-damper deflections and aileron inputs.

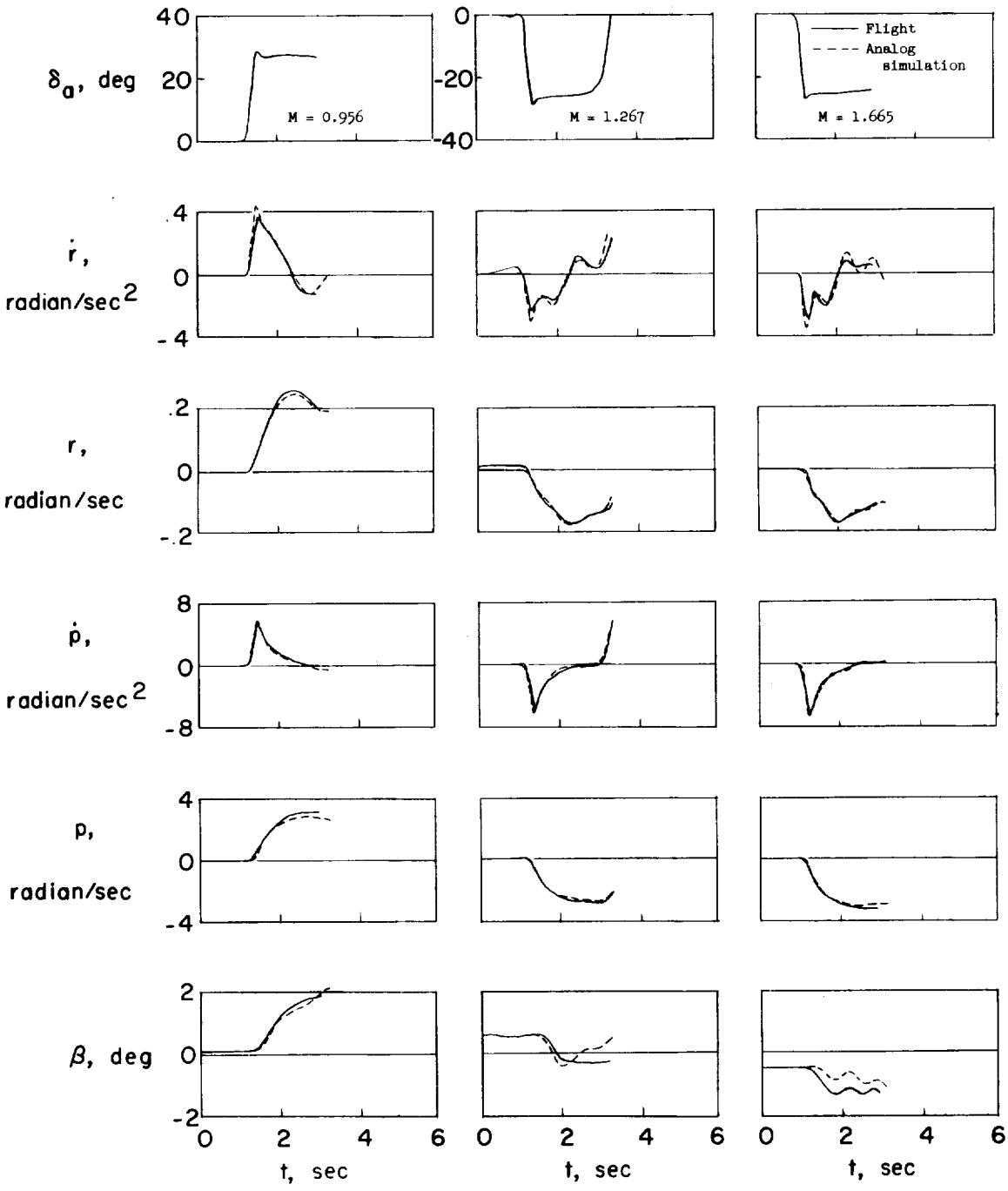

(b) Aileron deflection.

Figure 8.- Concluded.

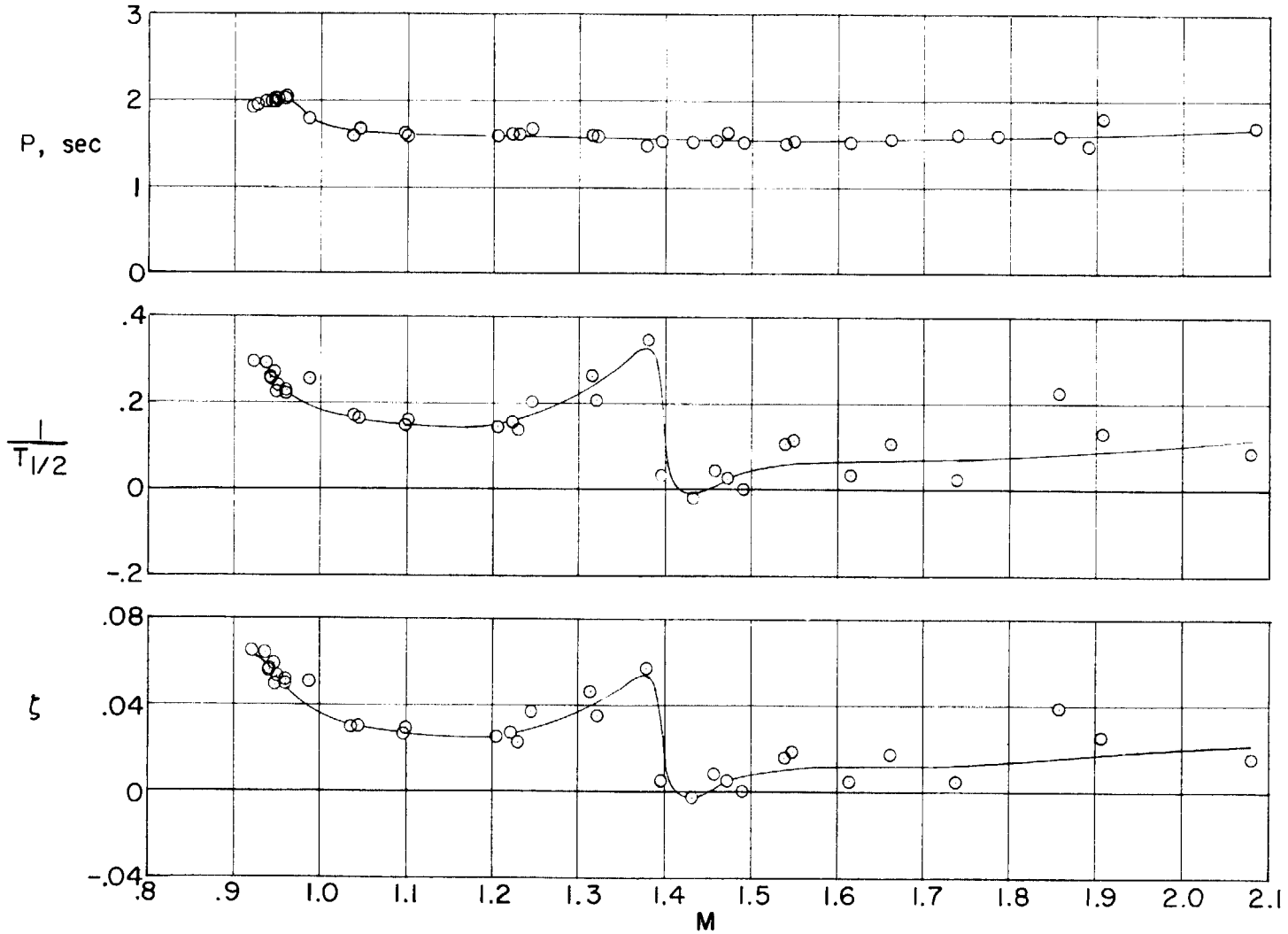

Figure 9.- Variation with Mach number of the lateral-directional period and damping characteristics of the test airplane.

CONFIDENTIAL

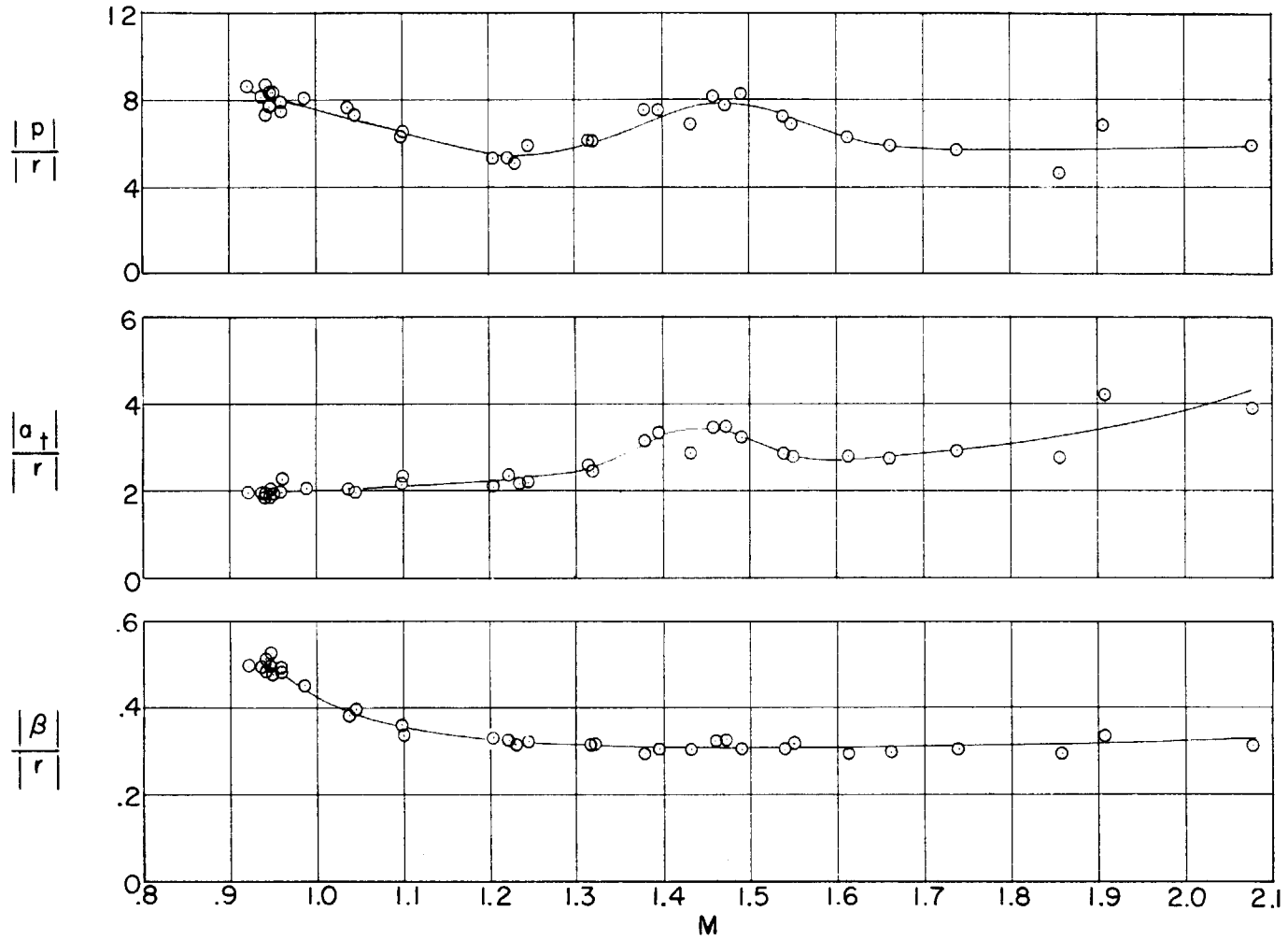

Figure 10.- Variation with Mach number of the amplitude ratios $\frac{|p|}{|r|}$, $\frac{|a_t|}{|r|}$, and $\frac{|\beta|}{|r|}$ of the test airplane at its natural frequency.

CONFIDENTIAL

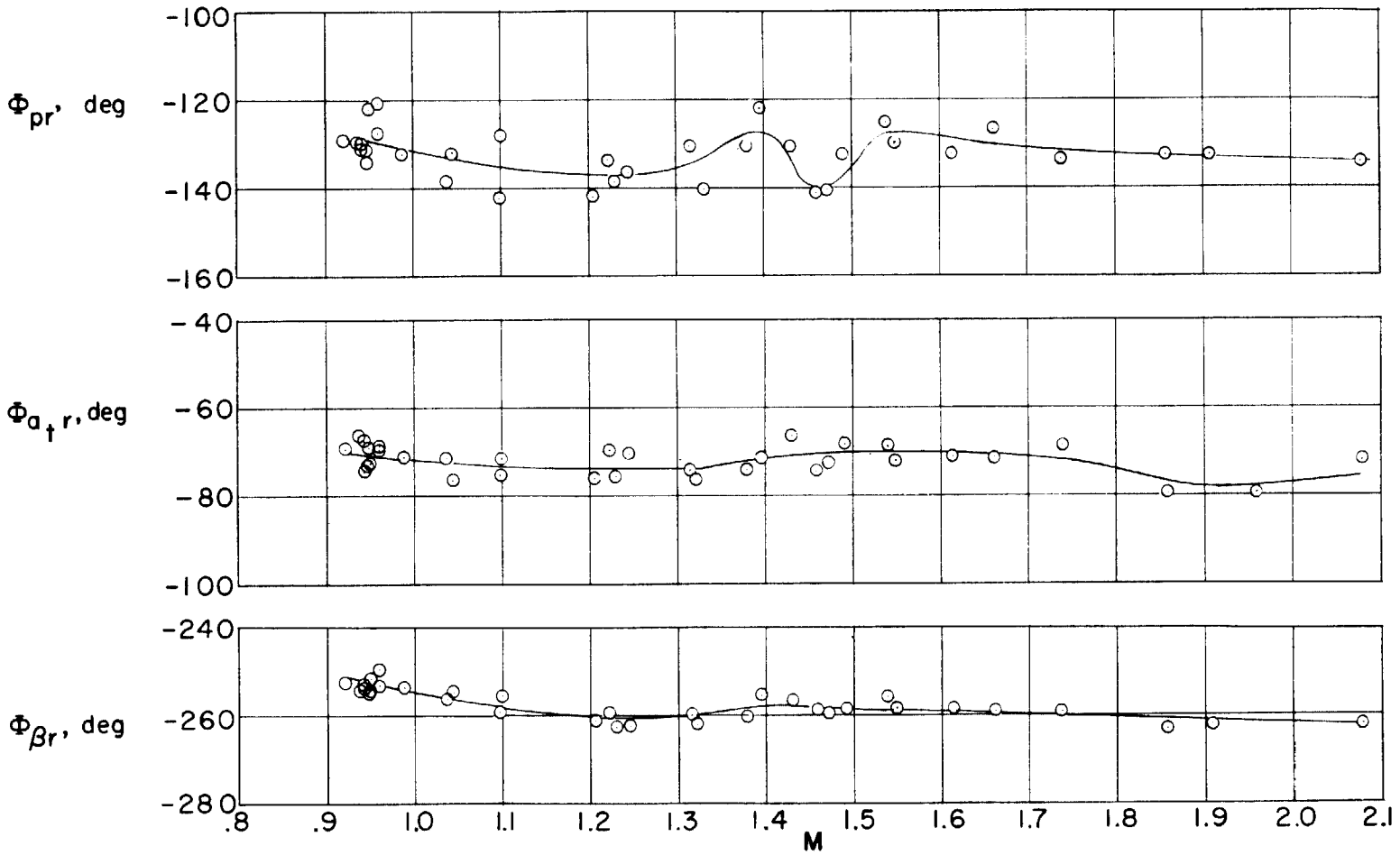

Figure 11.- Variation with Mach number of the phase angles Φ_{pr}, $\Phi_{a_t r}$, and $\Phi_{\beta r}$ of the test airplane at its natural frequency.

CONFIDENTIAL

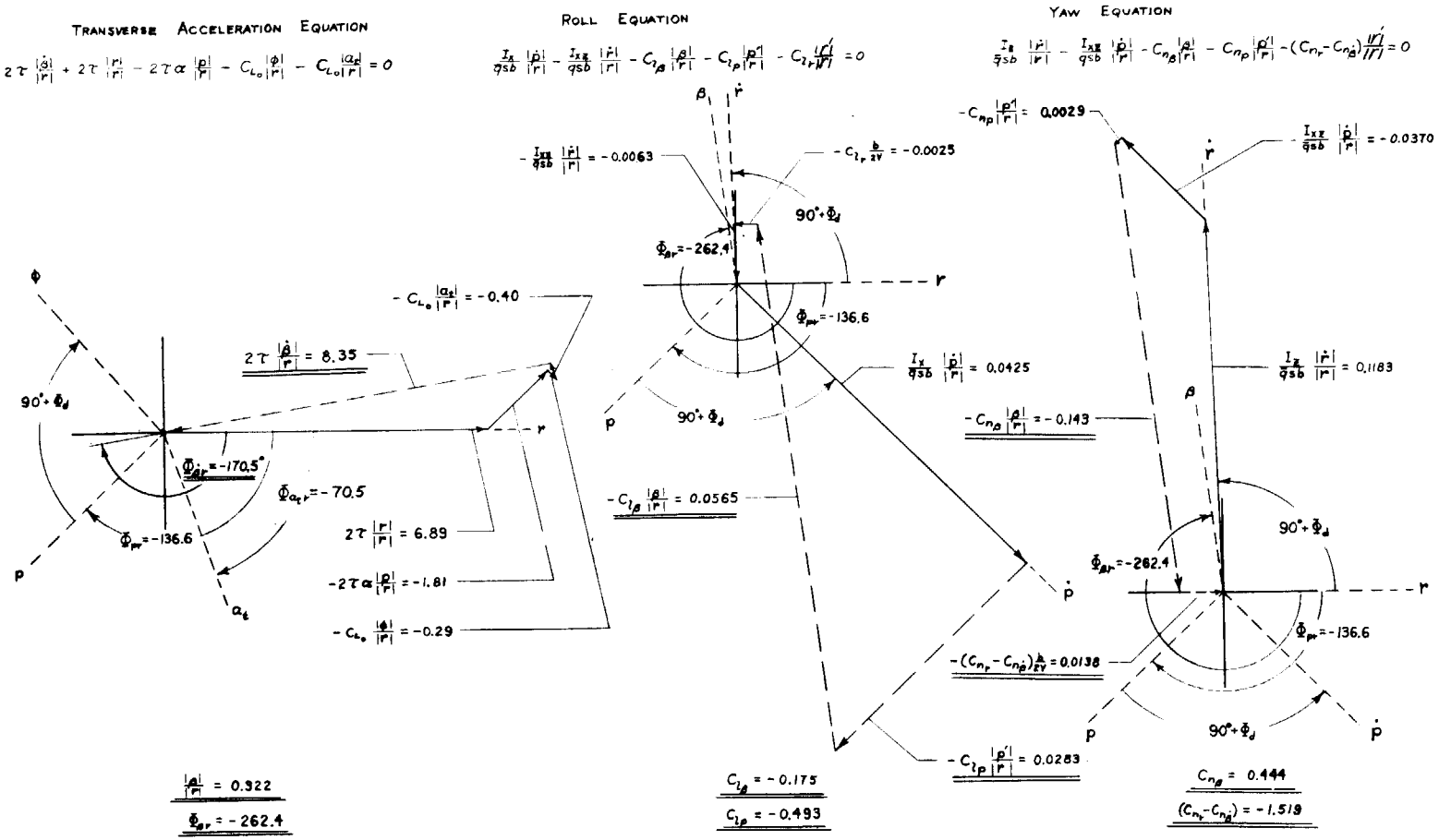

Figure 12.- Representative time-vector diagrams employed in the determination of the lateral-directional stability derivatives. $h_p \approx 40{,}000$ ft; M = 1.245.

CONFIDENTIAL

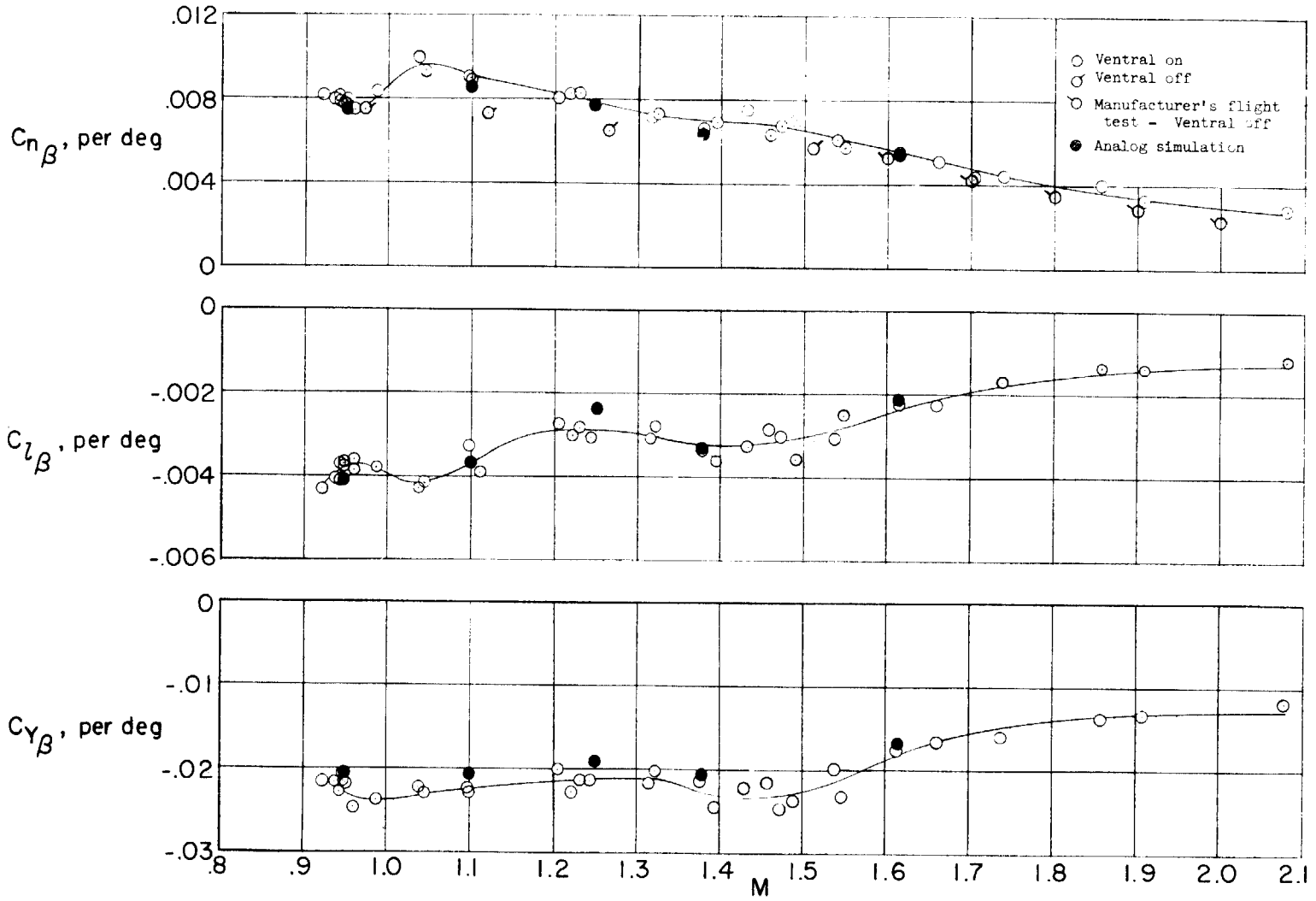

Figure 13.- Flight-determined static lateral-directional stability derivatives.

CONFIDENTIAL

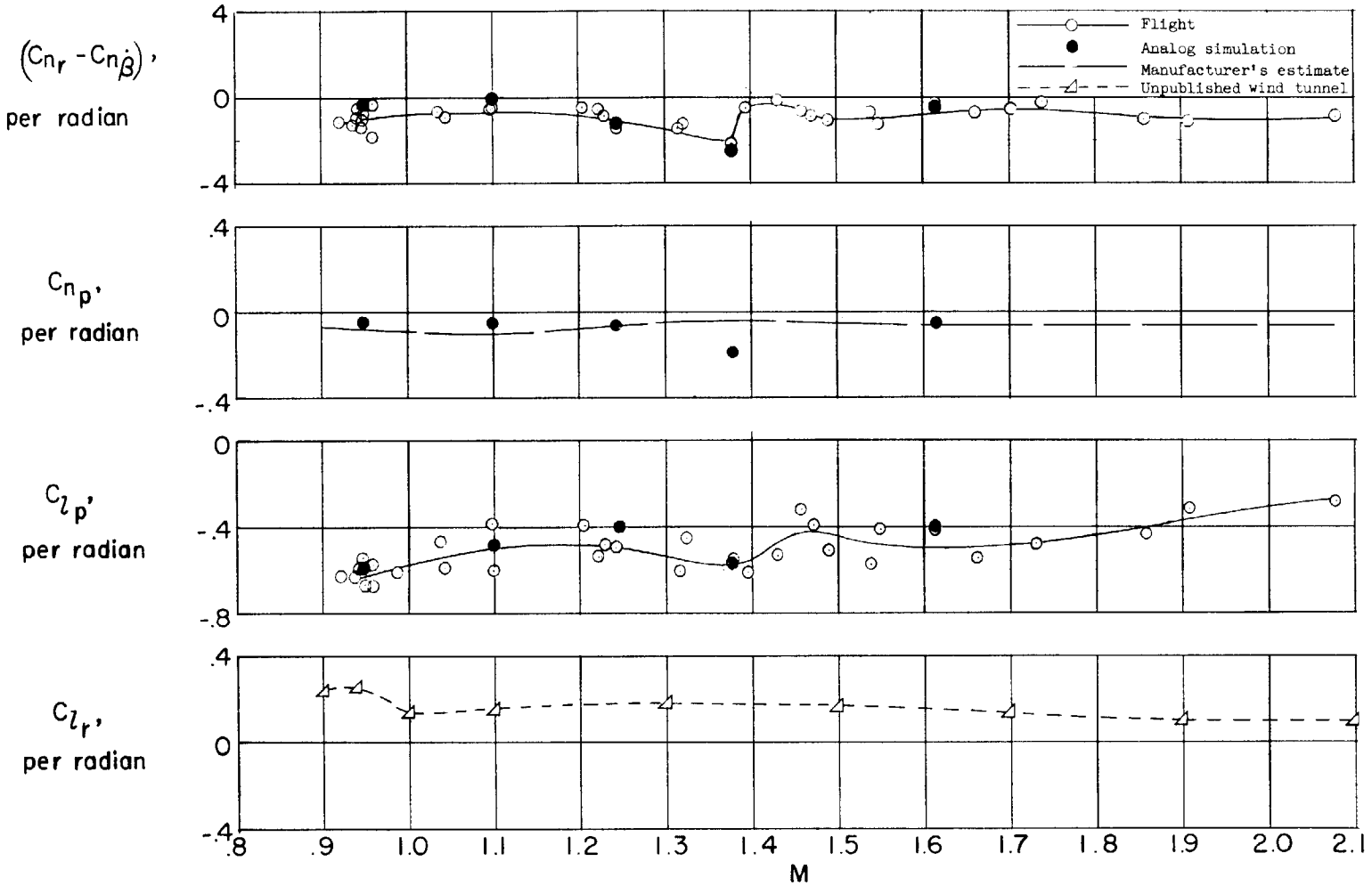

Figure 14.- Flight-determined dynamic lateral-directional stability derivatives.

CONFIDENTIAL

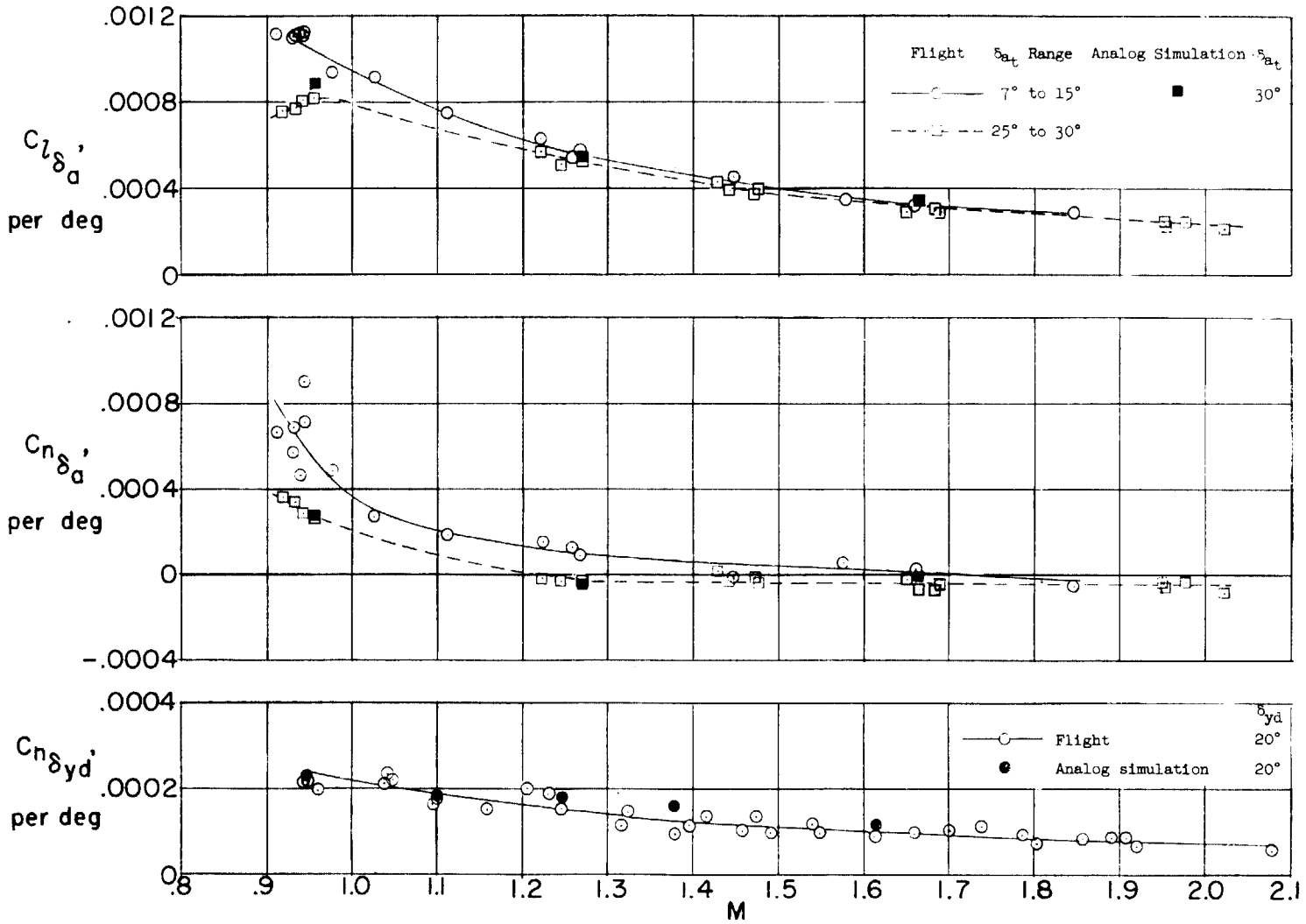

Figure 15.- Variation with Mach number of the flight-determined lateral-directional control-effectiveness derivatives.

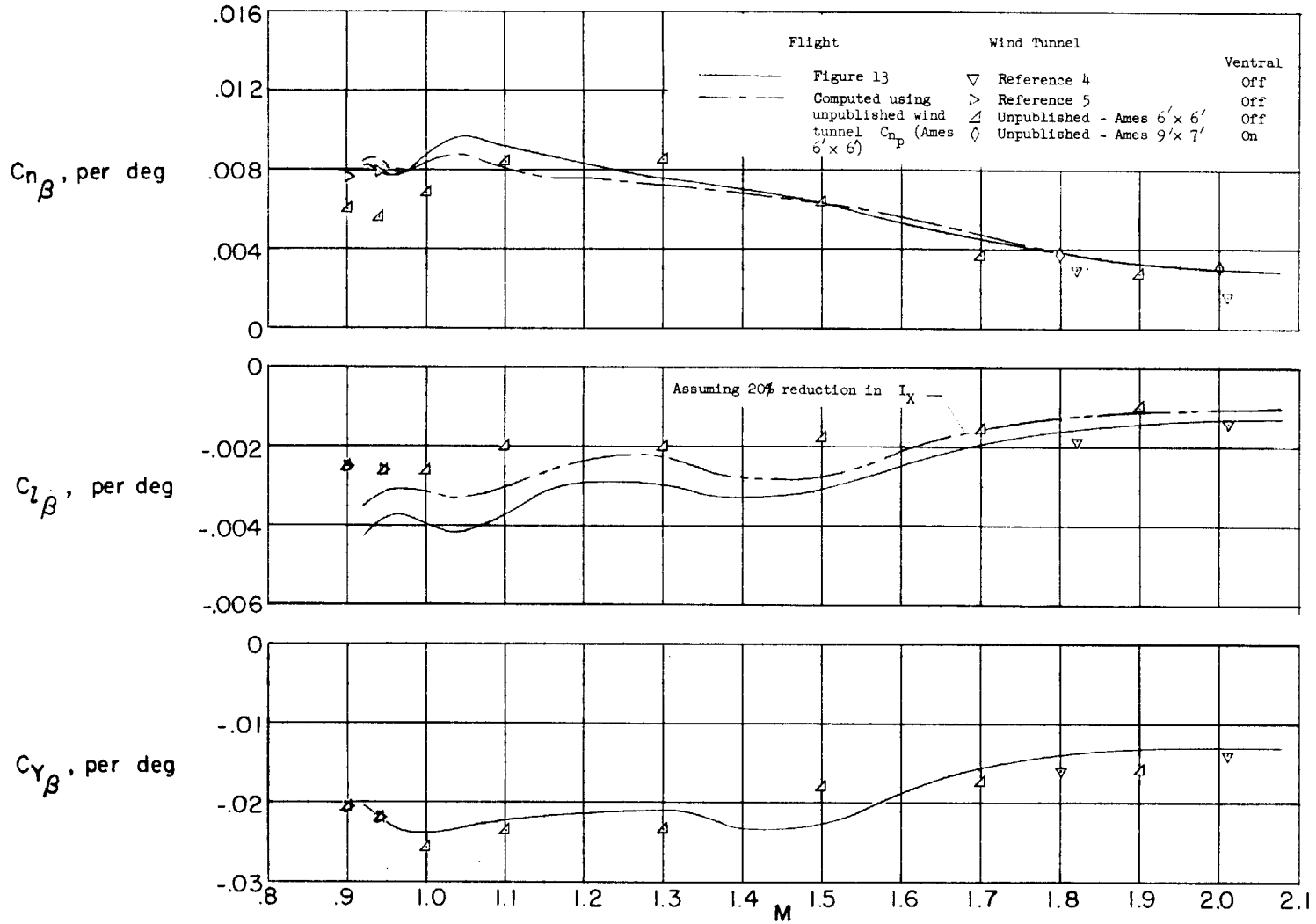

Figure 16.- Comparison of the flight-determined lateral-directional static stability derivatives with wind-tunnel results.

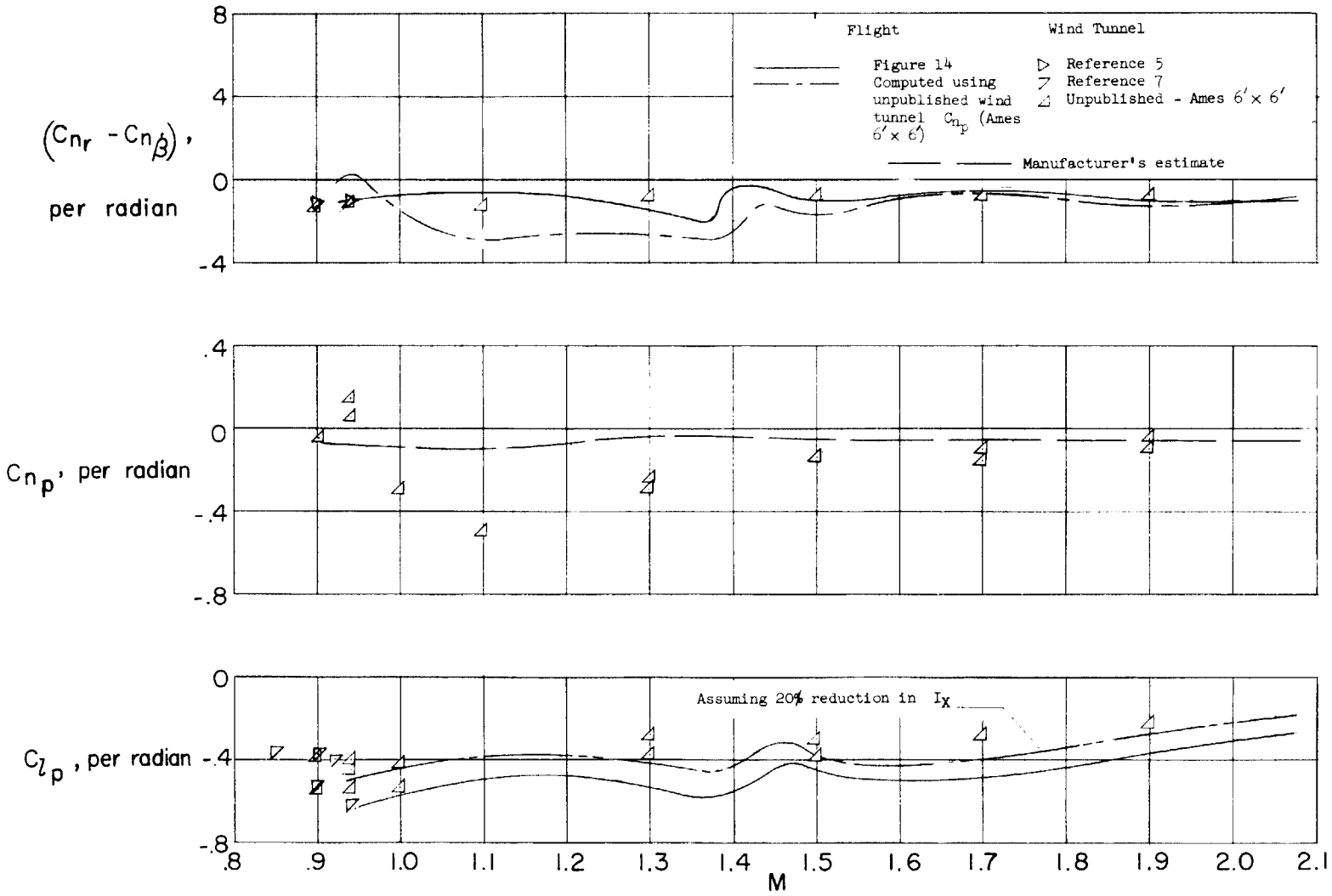

Figure 17.- Comparison of the flight-determined dynamic lateral-directional stability derivatives with wind-tunnel results.

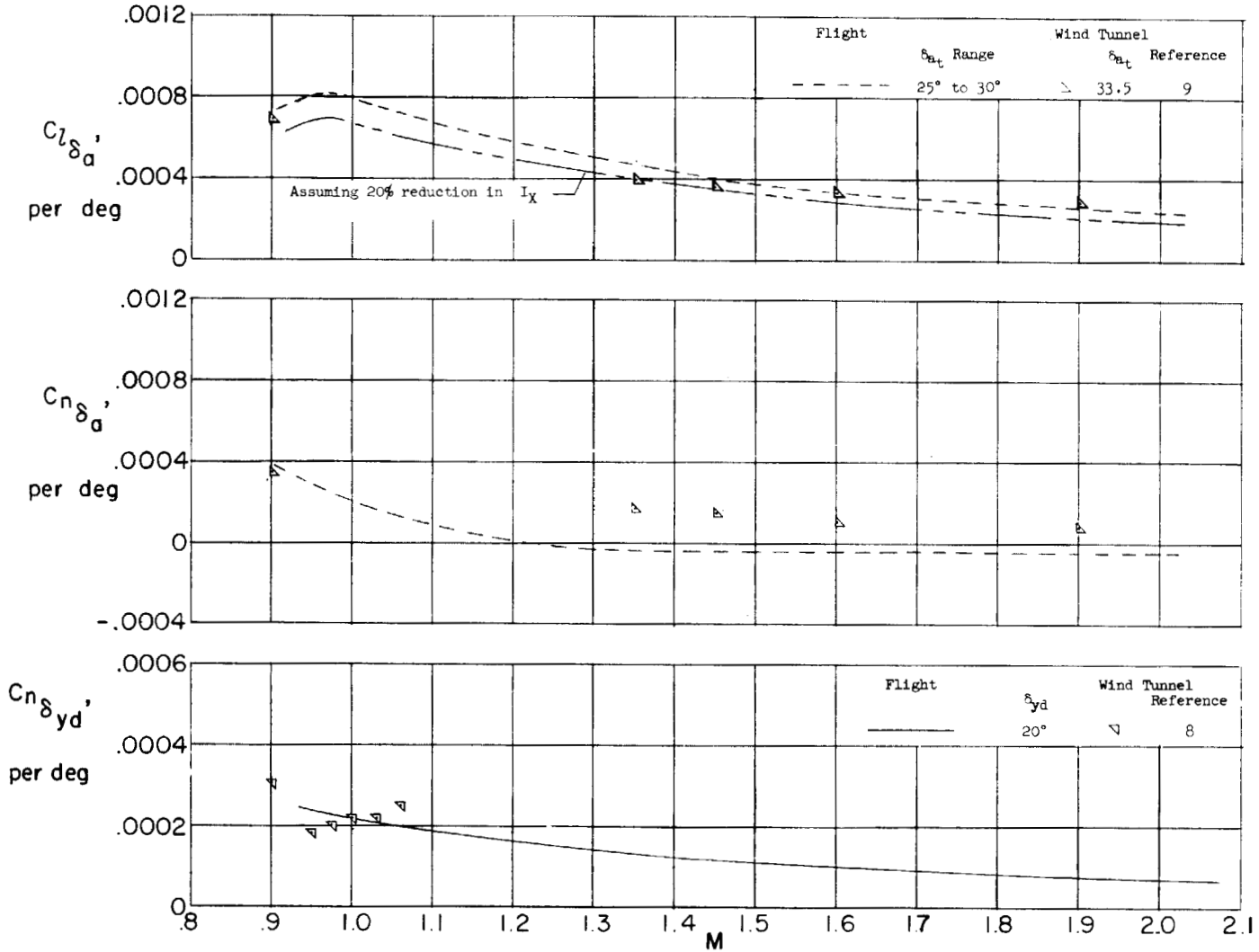

Figure 18.- Comparison of the flight-determined lateral-directional control-effectiveness derivatives with wind-tunnel results.